Bimodal Control of a Ca^{2+}-activated Cl^- Channel by Different Ca^{2+} Signals

Akinori Kuruma and H. Criss Hartzell

From the Department of Cell Biology, Emory University School of Medicine, Atlanta, Georgia 30322-3030

abstract Ca^{2+}-activated Cl^- channels play important roles in a variety of physiological processes, including epithelial secretion, maintenance of smooth muscle tone, and repolarization of the cardiac action potential. It remains unclear, however, exactly how these channels are controlled by Ca^{2+} and voltage. Excised inside-out patches containing many Ca^{2+}-activated Cl^- channels from *Xenopus* oocytes were used to study channel regulation. The currents were mediated by a single type of Cl^- channel that exhibited an anionic selectivity of $I^- > Br^- > Cl^-$ (3.6:1.9:1.0), irrespective of the direction of the current flow or $[Ca^{2+}]$. However, depending on the amplitude of the Ca^{2+} signal, this channel exhibited qualitatively different behaviors. At $[Ca^{2+}] < 1$ μM, the currents activated slowly upon depolarization and deactivated upon hyperpolarization and the steady state current–voltage relationship was strongly outwardly rectifying. At higher $[Ca^{2+}]$, the currents did not rectify and were time independent. This difference in behavior at different $[Ca^{2+}]$ was explained by an apparent voltage-dependent Ca^{2+} sensitivity of the channel. At +120 mV, the EC_{50} for channel activation by Ca^{2+} was approximately fourfold less than at −120 mV (0.9 vs. 4 μM). Thus, at $[Ca^{2+}] < 1$ μM, inward current was smaller than outward current and the currents were time dependent as a consequence of voltage-dependent changes in Ca^{2+} binding. The voltage-dependent Ca^{2+} sensitivity was explained by a kinetic gating scheme in which channel activation was Ca^{2+} dependent and channel closing was voltage sensitive. This scheme was supported by the observation that deactivation time constants of currents produced by rapid Ca^{2+} concentration jumps were voltage sensitive, but that the activation time constants were Ca^{2+} sensitive. The deactivation time constants increased linearly with the log of membrane potential. The qualitatively different behaviors of this channel in response to different Ca^{2+} concentrations adds a new dimension to Ca^{2+} signaling: the same channel can mediate either excitatory or inhibitory responses, depending on the amplitude of the cellular Ca^{2+} signal.

key words: ion channels • electrophysiology • ion channel gating • calcium signaling • ion transport

INTRODUCTION

Ca^{2+}-activated Cl^- channels play fundamental roles in physiological processes in many tissues, including secretion in airway epithelium (Wagner et al., 1991; Gray et al., 1995), repolarization of the cardiac action potential (Zygmunt, 1994; Kawano et al., 1995; Wang et al., 1995; Collier et al., 1996), regulation of vascular tone (Nelson et al., 1997; Yuan, 1997; Nilius et al., 1997a,b), modulation of photoreceptor light responses (Barnes and Deschenes, 1992), olfactory transduction (Kurahashi and Yau, 1994), neuronal excitability (DeCastro et al., 1997), regulation of platelet cell volume (Fine et al., 1994), and fast block to polyspermy in oocytes (Jaffe and Cross, 1986). Ca^{2+}-activated Cl^- channels may be involved in several human diseases, including cystic fibrosis and cardiac arrhythmias. Although defects in the CFTR Cl^- channel cause cystic fibrosis, upregulation of a Ca^{2+}-activated Cl^- current in the airway of CFTR knockout mice can compensate for the lack of CFTR and ameliorate the pathology in this mouse model (Clarke et al., 1994; Grubb et al., 1994). Furthermore, overexpression of CFTR in cultured airway epithelial cells from CF patients results in a decrease in Ca^{2+}-activated Cl^- current (Johnson et al., 1995). Ca^{2+}-activated Cl^- channels also play a role in the repolarization of the cardiac action potential and contribute to the transient outward current (I_{to}) (Zygmunt and Gibbons, 1991, 1992; Zygmunt, 1994; Zygmunt et al., 1998.). Recently, it has been shown that dogs which are genetically prone to cardiac sudden death have an abnormal I_{to} (Freeman et al., 1997), implying that Ca^{2+}-activated Cl^- channels might play a role in cardiac sudden death. Ca^{2+}-activated Cl^- channels also contribute to the transient inward current (Han and Ferrier, 1992, 1996), which is believed to trigger cardiac arrhythmias during Ca^{2+} overload (Berlin et al., 1989).

Despite the importance of Ca^{2+}-activated Cl^- channels in cell physiology, our understanding of the mechanisms of regulation and gating of these channels remains rudimentary. In different studies and cell types, Ca^{2+}-activated Cl^- currents behave differently. Often, these currents are voltage sensitive: they activate slowly on depolarization and deactivate on hyperpolarization (e.g., Cliff and Frizzell, 1990; Arreola et al., 1996; Nilius et al., 1997b; Anderson and Welsh, 1998), but in other studies the currents appear time and voltage independent (e.g., Xie et al., 1996; Collier et al., 1996). It is not

Address correspondence to H. Criss Hartzell, 1648 Pierce Dr., Department of Cell Biology, Emory University School of Medicine, Atlanta, GA 30322-3030. Fax: 404-727-6256; E-mail: criss@cellbio.emory.edu

J. Gen. Physiol. © The Rockefeller University Press • 0022-1295/2000/01/59/22 $5.00
Volume 115 January 2000 59–80
Released online 28 December 1999
http://www.jgp.org

known whether this difference is due to differences in regulation of the same type of channel, to different experimental protocols, or to different molecular species of Ca^{2+}-activated Cl^- channels. There is strong evidence in the literature for the existence of several classes of Ca^{2+}-activated Cl^- channels that are differentially regulated. The single channel conductances reported for Ca^{2+}-activated Cl^- channels range from 1 to 50 pS (Marty et al., 1984; Frizzell et al., 1986; Takahashi et al., 1987; Taleb et al., 1987, 1988; Marunaka and Eaton, 1990; Nishimoto et al., 1991; Klöckner, 1993; Collier et al., 1996; Schlenker and Fitz, 1996; Nilius et al., 1997a). Furthermore, Ca^{2+}-activated Cl^- currents that appear similar at the macroscopic level can be regulated differently; e.g., Ca^{2+}-activated Cl^- currents in T84 intestinal cells require CaMKII for activation, whereas those in rat parotid gland cells do not (Arreola et al., 1998). The cloning of a Ca^{2+}-activated Cl^- current has been reported (Cunningham et al., 1995; Gruber et al., 1998; Ji et al., 1998), but it seems unlikely that this is the same channel studied here because the single channel conductance (Takahashi et al., 1987) and pharmacology (Hartzell, unpublished observations) differ.

Xenopus oocytes have long been a model system for studying Ca^{2+}-activated Cl^- channels (Dascal, 1987) because these channels are the predominant channel type natively expressed in this cell and because they are expressed at extremely high levels (0.5 mA/cm^2). The *Xenopus* oocyte Ca^{2+}-activated Cl^- currents have been studied in considerable detail at the macroscopic level (see references in Yao and Parker, 1993, and Kuruma and Hartzell, 1999). The inward and outward Ca^{2+}-activated Cl^- currents are regulated differently: outward Cl^- current is activated at lower cytosolic [Ca^{2+}] than is inward Cl^- current (Kuruma and Hartzell, 1999). Although this difference in Ca^{2+} sensitivity could be explained by two different classes of Cl^- channels with different Ca^{2+} affinities (Boton et al., 1989; Hartzell, 1996; Kuruma and Hartzell, 1999), it could also be explained by a single class of Cl^- channel that exhibits voltage-dependent Ca^{2+} affinity (Yao and Parker, 1993). Because *Xenopus* oocytes have been such an important model system for the study of Ca^{2+}-activated Cl^- channels, we have begun a detailed investigation into the mechanisms of their regulation and gating. The purpose of the present investigation was to characterize quantitatively the regulation of *Xenopus* oocyte Ca^{2+}-activated Cl^- currents by Ca^{2+} and voltage in excised inside-out patches where cytosolic Ca^{2+} could be precisely controlled and to determine whether the macroscopic currents in *Xenopus* oocytes could be explained by a single class of Cl^- channels. We find that Ca^{2+}-activated Cl^- currents in *Xenopus* oocytes can be explained by a single class of channel that exists in multiple closed and open states. Channel opening absolutely requires Ca^{2+} and is independent of voltage, but channel closing is voltage sensitive. At low [Ca^{2+}], the probability of channel opening at hyperpolarized potentials is low because the rate of channel closure (voltage sensitive) is rapid relative to channel opening (Ca^{2+} sensitive). As [Ca^{2+}] is increased, the rate of channel opening dominates at all potentials and the current becomes voltage independent. These features define a new aspect of Ca^{2+} signaling, where a single effector molecule can behave qualitatively differently depending on the Ca^{2+} signal.

METHODS

Solutions

Solutions containing different free [Ca^{2+}] were made by the method of Tsien and Pozzan (1989). 0-Ca^{2+} solution contained 150 mM NMDG-Cl, 5.07 $MgCl_2$, 10 mM EGTA, and 10 mM HEPES, pH 7.3 with NMDG. High Ca^{2+} solution contained 150 mM NMDG, 4.12 mM $MgCl_2$, 10 mM Ca-EGTA, 10 mM HEPES, pH 7.3. The stock 100 mM Ca-EGTA solution was made by the pH-metric method described by Tsien and Pozzan (1989), except that NMDG was used to adjust pH. Working solutions having different free Ca^{2+} were prepared by mixing the 0-Ca^{2+} solution with the high-Ca^{2+} solution in various ratios. The free [Ca^{2+}] was calculated from the equation: $[Ca^{2+}] = K_d \times [\text{Ca chelator}]/[\text{free chelator}]$, where K_d is the K_d of the Ca^{2+} chelator, EGTA ($K_d = 1.0 \times 10^{-7}$ M at 24°C, pH 7.3, ionic strength 0.16 M, 4 mM Mg^{2+}). For solutions >1 μM free Ca, we sometimes used a relatively high-K_d chelator, 5,5′-dibromo-1,2-bis(2-aminophenoxy) ethane-*N*,*N*,*N*′,*N*′-tetraacetic acid ($K_d = 1.98 \times 10^{-6}$ M at 24°C, pH 7.3, ionic strength 0.16 M, 4 mM Mg^{2+}; Molecular Probes, Inc.), for better Ca^{2+} buffering. Free Mg^{2+} was always adjusted to 4 mM using the program MaxC 1.0 (http://www.stanford.edu/~cpatton/maxc.html; Bers et al., 1994). The calculated Ca^{2+} concentrations were confirmed in each solution by fura-2 (Molecular Probes, Inc.) measurements using an LS-50B luminescence spectrophotometer (Perkin-Elmer Corp.). For the low Cl^- pipet solution, Cl^- was replaced with aspartate. For anion permeability experiments, Cl^- was replaced by Br^- or I^-. NMDG-bromide and NMDG-iodide were made by titrating NMDG with hydrobromic and hydriodic acid, respectively. All reagents were purchased from Sigma Chemical Co. unless stated otherwise.

Isolation of Xenopus oocytes

Stage V–VI oocytes were harvested from adult *Xenopus laevis* females (Xenopus I) as described by Dascal (1987). Xenopus oocytes were anesthetized by immersion in Tricaine (1.5 g/liter). Ovarian follicles were removed, cut into small pieces, and digested in normal Ringer with no added calcium containing ~2 mg/ml collagenase type IA for 2 h at room temperature. The oocytes were extensively rinsed with normal Ringer, placed in L-15 medium (GIBCO BRL) and stored at 18°C. Oocytes were used 1–4 d after isolation. On the day of recording, oocytes were shaken in hypertonic solution (200 mM K-aspartate, 20 mM KCl, 1 mM $MgCl_2$, 10 mM EGTA, 10 mM HEPES, pH 7.2 with KOH) for 10–15 min to facilitate manual removal of the vitelline membrane, and then they were placed in normal Ringer solution until use.

Electrophysiological Methods

All recordings were performed using the inside out patch-clamp configuration with symmetrical Cl^- concentration except where noted. Patch pipets were made of borosilicate glass (Sutter Instrument Co.) pulled by a Model-2000 puller (Sutter Instrument

Co.), coated with Sylgard (Dow Corning Corp.) and fire polished. Patch pipets had resistances of 4–8 MΩ. They were filled with 0-Ca^{2+} solution (or in some experiments high-Ca^{2+} solution, with the same results). The bath was grounded via a 3 M KCl-agar bridge connected to a Ag-$AgCl^-$ reference electrode. After obtaining a giga-ohm seal, the patch was excised into 0-Ca^{2+} solution. For routine experiments, solution changes were performed by gravity feed of the 300-μl chamber at ~10 ml/min using a perfusion manifold (MP-8; Warner Instruments). Solution exchange occurred in ~5 s. See below for a description of the method for rapid solution changes. The seals were consistently >50 GΩ and root mean square noise was <0.2 pA. The seals typically lasted for 20–60 min. Patches were generally obtained from the animal hemisphere because Ca^{2+}-activated Cl^- currents are concentrated here (Gomez-Hernandez et al., 1997; Machaca and Hartzell, 1998). The amplitude of the Ca^{2+}-activated Cl^- currents varied significantly between patches as well as between oocytes from different batches. Liquid junction potentials were measured for each experimental solution as described by Neher (1992) and corrected after the recordings. Instantaneous currents were measured 1 ms after the onset of the voltage pulse.

Data were usually acquired by an Axopatch 200B (or 200A) amplifier that was controlled by Clampex 7.0.1 via a Digidata 1200 analogue-to-digital and digital-to-analogue converter (Axon Instruments). For some experiments, the data was acquired by Curcap 3.0 (W. Goolsby, Emory University, Atlanta, GA) and voltages were delivered by a Challenger DB stimulator (W. Goolsby). Experiments were conducted at room temperature (20–24°C).

Ca^{2+} Concentration Jump Experiments

Rapid changes in [Ca^{2+}] were made using a system similar to that described by Naranjo and Brehm (1993). In brief, the excised patch was placed at the confluence of two solution streams that were switched by a solenoid (225P072-11; Neptune Research and Development, Inc.) controlled by the Challenger stimulator (W. Goolsby). The solutions flowed at a rate of 5–10 ml/min from 0.5-mm–diameter orifices. As shown in results, it was possible to switch between two different solutions in <5 ms.

Display and Analysis of Data

For the calculations and graphical presentation, we used Origin 5.1 software (Microcal Software, Inc.). Exponential fits for activation and deactivation kinetics of current traces were usually performed using the iterative Levenberg-Marquardt algorithm in Origin. For some experiments, we used the Pade-LaPlace algorithm for fitting exponentials (Yeramian and Claverie, 1987; Bajzer et al., 1989) (Xcalcwin; Patrick Lechene, University of Paris, Chatenay-Malabry, France). Results are presented as mean ± SEM, and *n* refers to the number of patches in each experiment.

RESULTS

Activation of Currents in Excised Patches by Cytosolic Ca

Fig. 1 shows typical current records from an inside-out excised patch from a *Xenopus* oocyte containing many Ca^{2+}-activated Cl^- channels. Both cytosolic and extracellular solutions contained 150 mM NMDG-Cl, 4 mM Mg^{2+}, 10 mM EGTA, and 10 mM HEPES, pH 7.3 with NMDG. The cytosolic side of the patch was exposed to this solution with Ca^{2+} · EGTA added to adjust the free Ca^{2+} concentration to values of <10 or 600 nM. The patch was held at 0 mV and stepped to V_m between

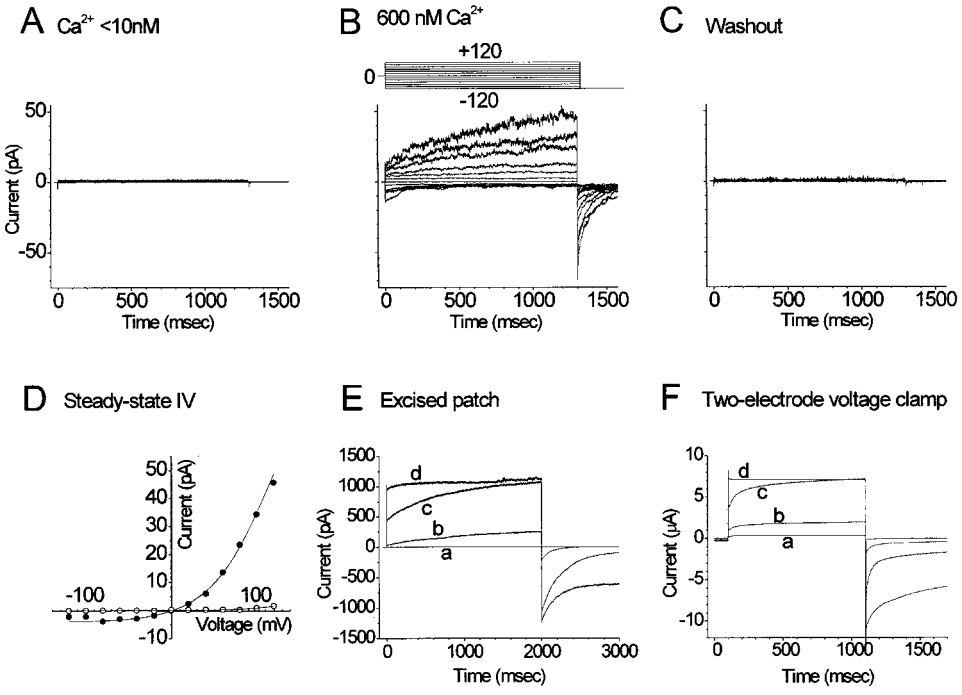

Figure 1. Activation of Ca^{2+}-activated Cl^- currents in an excised inside-out patch from a *Xenopus* oocyte. The cytosolic face of an excised inside-out patch was exposed to NMDG-Cl solutions containing <10 nM (A and C) or 600 nM (B) Ca^{2+}. The patch was voltage clamped by stepping from a holding potential of 0 mV to various potentials between +120 and −120 mV for 1.3 s, followed by a 0.3-s step to −120 mV (voltage protocol is shown above B). The largest outward current corresponds to the +120-mV pulse. (D) Steady state current–voltage relationship for excised patch current. The currents at the end of the 1.3-s pulse from B were plotted versus membrane potential. ●, 600 nM Ca^{2+}; ○, ,10 nM Ca^{2+}. (E–F) Comparison of currents in excised patch with whole-cell currents. (E) The "excised-patch" current was recorded with symmetrical Cl^- at a transmembrane voltage of +200 mV. The cytosolic face of the patch was exposed to (a) <10 nM, (b) 460 nM, (c) 1. 1 μM, and (d) 1.8 μM Ca^{2+}. (F) The "whole-cell" current ($I_{Cl1\text{-}S}$) was recorded in an intact oocyte by two-electrode voltage clamp after injection of (a) none, (b) 320 pmol Ca^{2+} (10 s after injection), (c) 690 pmol Ca^{2+} (10 s after injection), and (d) 690 pmol Ca^{2+} (20 s after injection). The transmembrane voltage was +80 mV and extracellular Cl^- was 134 mM. Tail currents for both E and F were recorded at −120 mV.

−120 and +120 mV for 1.3 s, and then stepped to −120 mV for 0.3 s. At <10 nM Ca^{2+}, no currents were observed (Fig. 1 A). In contrast, at 600 nM Ca^{2+}, large sustained outward currents in response to depolarizing steps and deactivating inward tail currents in response to hyperpolarizing steps were observed (Fig. 1 B). Very little steady state inward current was observed at negative potentials. The effect of Ca^{2+} was reversible (Fig. 1 C). The outward currents at 600 nM Ca^{2+} were composed of a small instantaneous time-independent component and a large slowly activating time-dependent component. At +120 mV, the outward current at the end of the pulse was ~50 pA in this experiment, but ranged from ~20 to ~500 pA in different patches.

This Ca^{2+}- and voltage-sensitive current strongly resembled the outward Cl^- current activated by Ca^{2+} released from internal stores in response to IP_3 injection in intact oocytes. This current, called $I_{Cl1\text{-}S}$, has previously been extensively characterized using two-microelectrode voltage clamp (Hartzell, 1996; Kuruma and Hartzell, 1999). The waveforms of $I_{Cl1\text{-}S}$ and the excised patch currents are very similar (Fig. 1, E–F) and both currents exhibit strongly outwardly rectifying steady state current–voltage relationships (Fig. 1 D).

The Ca^{2+}-activated Currents Are Carried by Cl^- Ions

These currents were carried by Cl^- ions (Fig. 2). In this experiment, the instantaneous current–voltage relationship of the current was determined by measuring the amplitude of tail currents at different potentials after a depolarizing step to +120 mV with 160 mM Cl^- on both sides of the membrane (Fig. 2 A) or with 40 mM Cl^- in the bath and 160 mM Cl^- in the pipet (Fig. 2 B). In this experiment, the reversal potential of the current shifted +38.1 mV upon reducing extracellular [Cl^-]. On average, the reversal potential shifted +38.0 mV (symmetric Cl^- E_{rev} = 0.1 ± 0.43 mV, n = 18; asymmetric Cl^- E_{rev} = +39.0 ± 0.27 mV, n = 9). This shift was very close to the +36.3-mV shift predicted by the Goldman-Hodgkin-Katz equation. We conclude that this current in the excised patch corresponds to the Ca^{2+}-activated Cl^- current $I_{Cl1\text{-}S}$ we have described in intact oocytes because they are both activated by Ca^{2+}, carried by Cl^-, and have similar waveforms and steady state current–voltage relationships.

Voltage Dependence of Ca^{2+}-activated Cl^- Current at Different [Ca^{2+}]

Although the channel rectified strongly and activated/deactivated slowly with voltage pulses at low [Ca^{2+}], the behavior was dramatically different at higher [Ca^{2+}]. Fig. 3, A–F, shows a series of current traces from an excised patch exposed to different cytosolic [Ca^{2+}] from <10 nM to 2 μM Ca^{2+}. At [Ca^{2+}] > 1 μM, the current traces had very different waveforms than they did at lower [Ca^{2+}]. As the [Ca^{2+}] was increased, the outward current became increasingly dominated by the time-independent component. The current became essentially instantaneous at 2 μM Ca^{2+}. Also, rectification decreased with increasing Ca^{2+} concentration. At 2 μM Ca^{2+}, there were approximately equal amounts of steady state inward and outward currents at +120 and −120 mV (Fig. 3 E). Fig. 3 G shows that the steady state current–voltage relationship changed from outwardly

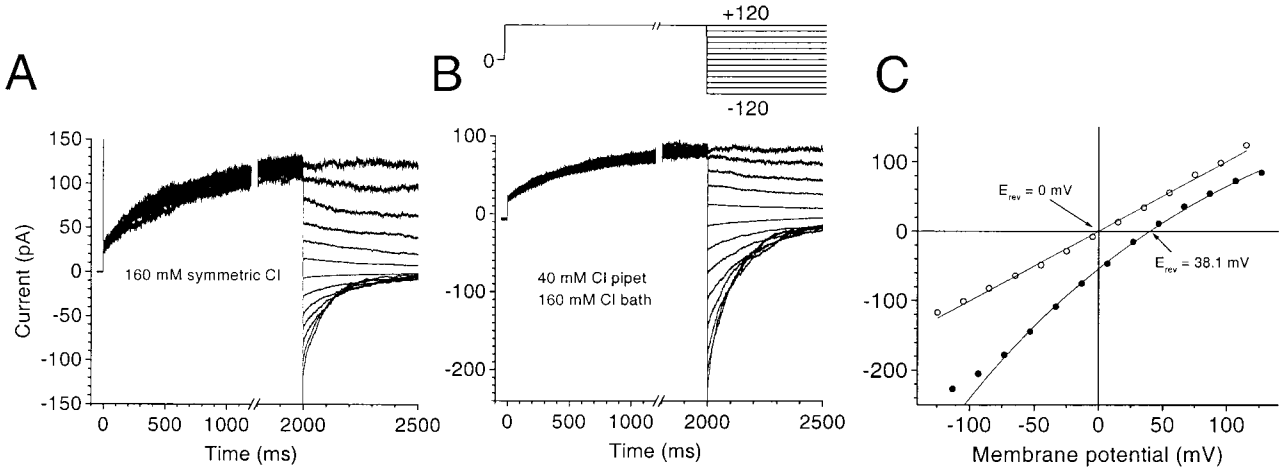

Figure 2. Excised patch currents are Cl^- currents. The reversal potential of the Ca^{2+}-activated currents recorded in inside-out patches was determined by measuring the instantaneous current at different potentials following a depolarizing step to +120 mV (voltage protocol is shown above B). The pipet solution contained either 160 (A) or 40 (B) mM Cl^-. The bath solution contained 160 mM Cl^-. (C) Instantaneous current–voltage relationship. The amplitudes of the tail currents were plotted versus the membrane potential for symmetric 160 mM Cl^- (○) or for 40 mM Cl_o–160 mM Cl_i (●). The reversal potential shifted from 0 to +38.1 mV with the reduction in extracellular Cl. The shift for a Cl-selective channel predicted by the Goldman-Hodgkin-Katz equation is +35.2 mV.

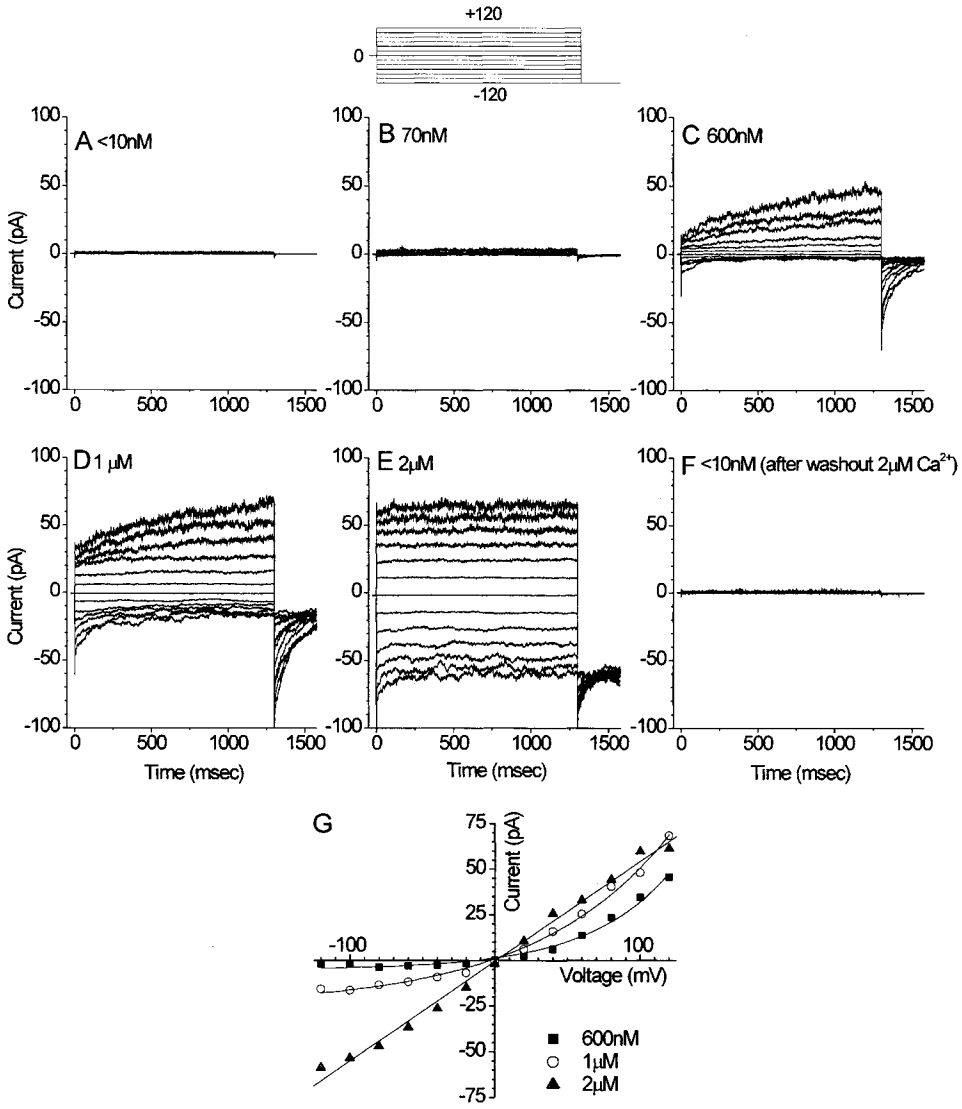

Figure 3. Ca^{2+} dependence of Cl^- currents in a single excised patch. The cytosolic face of an excised patch was exposed to solutions with different free [Ca^{2+}]: A, <10 nM Ca^{2+}; B, 70 nM Ca^{2+}; C, 600 nM Ca^{2+}; D, 1 μM Ca^{2+}; E, 2 μM Ca^{2+}; and F, <10 nM Ca^{2+} (after washing out 2 μM Ca^{2+}). The patch was voltage clamped by stepping to various potentials between +120 and −120 mV for 1.3 s from the holding potential of 0 mV, followed by a step to −120 mV for 0.3 s (protocol shown above B). (G) Steady state current–voltage relationships of currents at 600 nM Ca^{2+}, 1 μM Ca^{2+}, and 2 μM Ca^{2+}.

rectifying at <1 μM Ca to linear at >1 μM Ca^{2+}. This behavior resembled the behavior of Ca^{2+}-activated Cl^- currents activated by injecting different concentrations of Ca^{2+} into oocytes (Kuruma and Hartzell, 1999): with small injections of Ca, a time-dependent outward current was observed, whereas larger injections stimulated both inward and outward time-independent currents. These data show that, depending critically on [Ca^{2+}], the current exhibited qualitatively different rectification properties and waveforms.

The voltage dependencies of the currents at different [Ca^{2+}] were determined by plotting the conductance versus membrane potential. Conductance was determined by measuring the instantaneous currents at −120 mV after pulses to various potentials (voltage protocol as shown in Fig. 3) and dividing by the driving force (−120 mV). Fig. 4 A shows the average conductance–voltage curves (n = 4–13 different patches). Increasing [Ca^{2+}] over a rather narrow range, between 0.1 and 1 μM, shifted the conductance–voltage relationship strongly in the leftward direction and also significantly decreased the voltage dependence (slope). At the highest [Ca^{2+}] examined, the currents exhibited little or no voltage dependence within the voltage range tested.

The reader will notice that at 2.2 μM Ca^{2+} the conductance at depolarized potentials was less than the conductance at 1 μM Ca^{2+}. This was due to a spontaneous decrease in current amplitude with time (rundown). This rundown phenomenon was irreversible and Ca^{2+} dependent. The rate and magnitude of rundown were variable from patch to patch. For example, rundown was not obvious in Fig. 3, but usually at [Ca^{2+}] > 1 μM the current decreased exponentially to 50% of its initial value in 3–10 min. Patches in which rundown occurred rapidly were discarded from analysis, but otherwise we have not attempted to correct for rundown in any of the experiments shown here.

Quantitative analysis of the data was also compro-

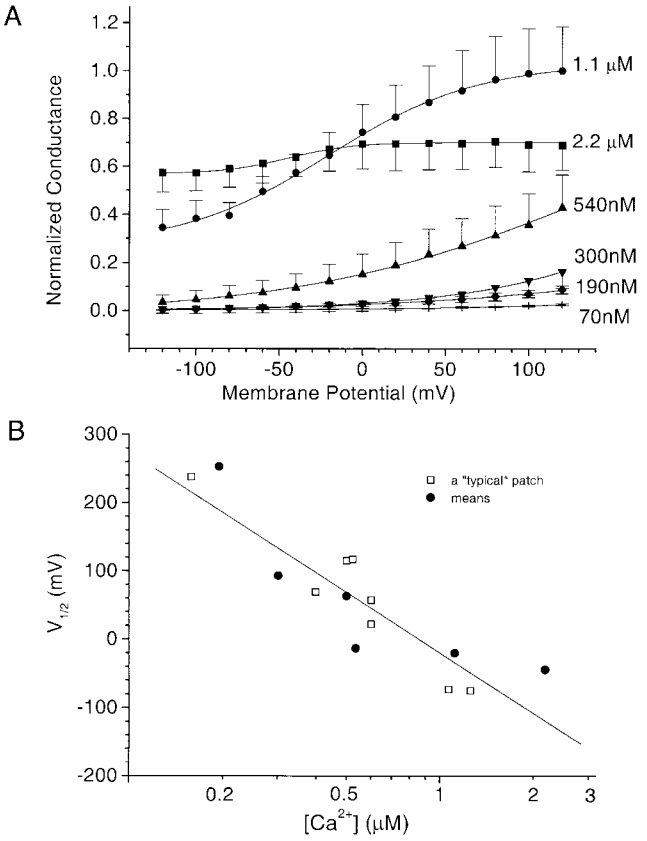

Figure 4. Voltage dependence of Ca^{2+}-dependent conductance. The voltage protocol was the same as in Fig. 3, but conductance was calculated by dividing the tail currents at −120 mV by the driving force, and then normalizing the data to the maximum conductance at +120 mV at 1.1 μM Ca^{2+} (∼0.5 nS). (A) Average of experiments at 2.2 μM Ca^{2+} ($n = 5$), 1.1 μM Ca^{2+} ($n = 4$), 540 nM Ca^{2+} ($n = 13$), 300 nM Ca^{2+} ($n = 12$), 190 nM Ca^{2+} ($n = 5$), and 70 nM Ca^{2+} ($n = 11$). The solid curves are fits to the Boltzmann equation. (B) Plot of the estimate of $V_{1/2}$ vs. $[Ca^{2+}]$. □, typical patch; ●, averages from A.

mised by the fact that it was usually not possible to maintain patches at voltages greater than ±120 mV, and the maximum our amplifier would deliver was ±200 mV, but voltages beyond this range were required to obtain the maximum and minimum conductances. Nevertheless, to estimate the voltage dependence, the available data for each $[Ca^{2+}]$ were fitted to the Boltzmann equation (Hille, 1992): $G = G_{max}\ (1/\{1 + \exp[-(V_m - V_{1/2})zF/RT]\}) + a$. Despite the limited voltage range, the fits were quite good. In the range of $[Ca^{2+}]$ where the data were most complete (between 0.5 and 1 μM), z, which is an estimate of the total gating charge movement, was ∼0.5. To evaluate the voltage dependence of the current at different $[Ca^{2+}]$, we assumed that z was the same at all $[Ca^{2+}]$, and estimated $V_{1/2}$ from the best fit. Fig. 4 B shows the estimated $V_{1/2}$ for the average of all patches. These data suggest that $V_{1/2}$ changes ∼295 mV for a 10-fold change in $[Ca^{2+}]$.

The Voltage-dependent Step Is after the Ca^{2+}-dependent Step

Fig. 4 has shown that at 2.2 μM Ca^{2+} the channel cannot be closed by voltages as negative as −120 mV and that at ∼10 nM Ca^{2+} the channel cannot be opened by voltages as positive as +120 mV. This suggests that channel opening is Ca^{2+} dependent and that the voltage-sensitive step is after Ca^{2+} binding. Fig. 5 extends the voltage range and shows that the channel cannot be closed by voltages even as negative as −200 mV. An excised patch was held at negative potentials for 10 s, and then stepped to +120 mV to measure the instantaneous current, to determine whether negative potentials could deactivate the current completely. At 500 nM Ca^{2+} (Fig. 5, A and B), a small, but significant outward current (30 pA) was recorded upon stepping from −100 to +120 mV. Increasing the holding potential to −200 mV had no significant effect on the magnitude of the instantaneous current. Thus, even at this intermediate $[Ca^{2+}]$, it was not possible to close the channels by strong depolarization. At 1 μM Ca^{2+} (Fig. 5, C and D), the currents were larger, but their amplitudes were not significantly reduced by increasing the holding potential from −160 to −200 mV. From these results, it is clear that channel opening is not voltage gated and that voltage only modulates the current amplitude. Rather, channel opening is strictly dependent on Ca^{2+} and the voltage sensitivity must occur at a later step.

Voltage-dependent Ca^{2+} Affinity of the Ca^{2+}-activated Cl Current

To analyze the voltage dependence of the current quantitatively, it was necessary to obtain recordings in the absence of significant rundown. Because rundown was Ca^{2+} dependent, we minimized rundown by reducing the amount of time the patch was exposed to Ca^{2+}. This was accomplished by using rapid solution changes that introduced Ca^{2+} only during voltage-clamp trials and by using voltage-clamp trials having fewer episodes than those used in the previous figures. Using this approach, a few patches were obtained in which rundown was <10% during the time (∼7–10 min) required to obtain a complete set of current–voltage curves at five different Ca^{2+} concentrations. To assess the amount of rundown, the maximal current at 120 mV was measured at the start of the experiment ($I_{INITIAL}$) during a brief (∼10 s) exposure to 40 μM Ca^{2+}. The patch was then returned to <10 nM Ca^{2+} solution, except during the voltage clamp trials, when it was exposed to different $[Ca^{2+}]$ (from 170 nM to 40 μM). The amplitude of the current at 120 mV during the last voltage clamp trial in 40 μM Ca^{2+} (I_{FINAL}) was compared with $I_{INITIAL}$. In the case of the patch illustrated in Fig. 6 A, $I_{INITIAL}$ and I_{FINAL} were virtually identical. Fig. 6 B is a plot of conductance versus V_m at different $[Ca^{2+}]$. Comparison

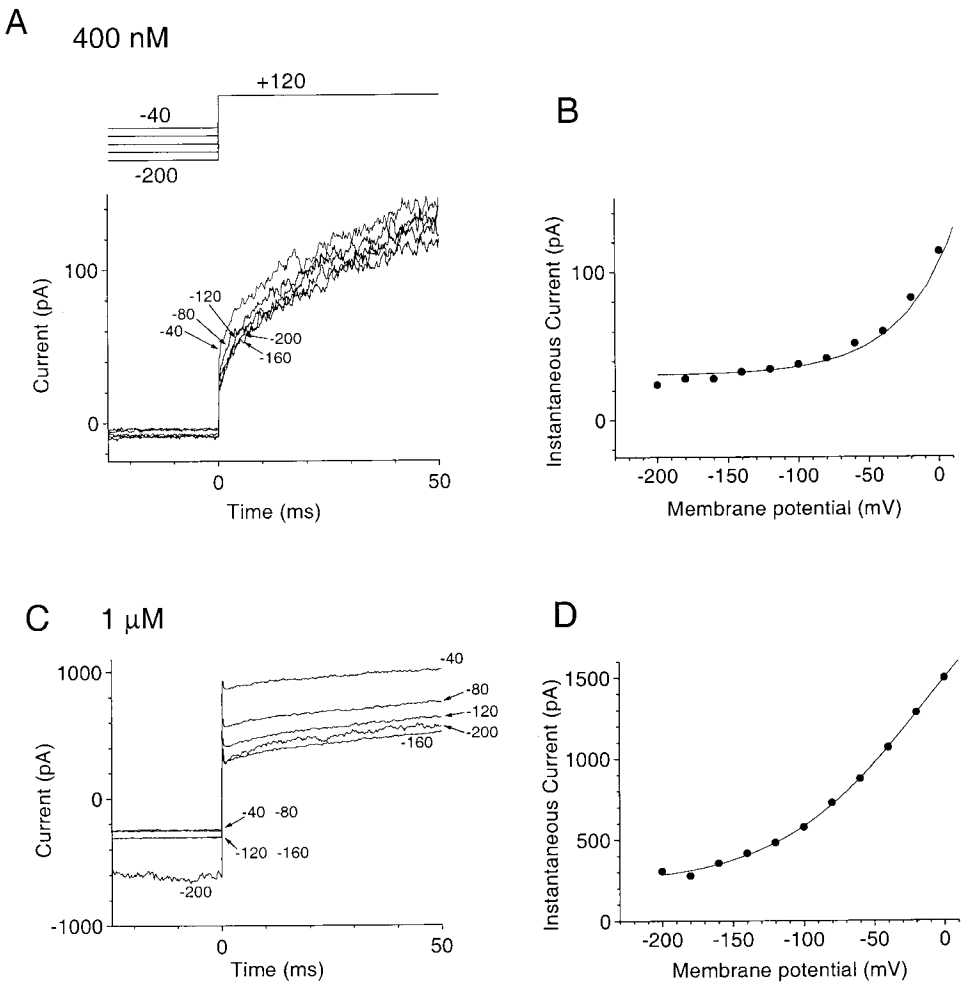

Figure 5. Hyperpolarization cannot turn off currents activated by Ca^{2+}. Excised patches were exposed to 500 nM Ca^{2+} (A and B) or 1 μM Ca^{2+} (C and D). The membrane potential was held at various values between −200 and 0 mV. The instantaneous currents at +120 mV were measured to determine the conductance activated at the preceding voltage. At both [Ca^{2+}], hyperpolarization to −200 mV was not able to inactivate the Ca^{2+}-activated current. Only selected traces are shown in A and C for clarity.

of this plot to the averages in Fig. 4 A shows that the general features and conclusions derived from Fig. 4 are valid, despite the presence of rundown.

To determine the voltage dependence of the Ca sensitivity of the channel, we plotted the amplitude of the tail currents versus [Ca^{2+}] for each voltage (Fig. 6 C), and the data were fitted to the Hill equation. This analysis shows that the apparent affinity of the channel for Ca^{2+} decreased approximately fourfold from 4 μM at −120 mV to 0.9 μM at +120 mV. The Hill coefficient ranged from 3.2 to 2.5 over the same voltage range (Fig. 6 D). This analysis assumes that 40 μM Ca^{2+} activated the current maximally. This assumption was tested in other patches by comparing the amplitudes of the currents in 40 and ~900 μM Ca^{2+}. The steady state current–voltage curves were the same at these two Ca^{2+} concentrations (Fig. 6 E).

The mean data from all patches including those exhibiting rundown (Fig. 6 F) were consistent with the conclusions obtained from the single patch in Fig. 6, A–D. Because of rundown at high [Ca^{2+}], data for [Ca^{2+}] > 1.1 μM were not included when fitting the mean data to the Hill equation. This limitation plus the presence of variable amounts of rundown at lower [Ca^{2+}] resulted in a smaller quantitative dependence of the apparent K_d on voltage: the mean apparent K_d differed only twofold between +120 and −120 mV (Fig. 6 F), whereas the champion patch (Fig. 6, A–D) exhibited a fourfold difference.

The finding that the Hill coefficient was >1 suggested that more than one Ca^{2+} ion bound to the channel to activate it. This suggests the existence of multiple Ca^{2+}-liganded closed states in a voltage-dependent equilibrium with Ca^{2+}-liganded open states. We propose Scheme I to describe the data.

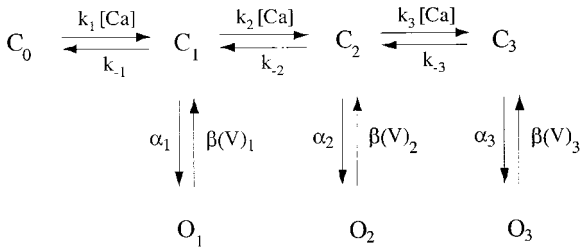

(SCHEME I)

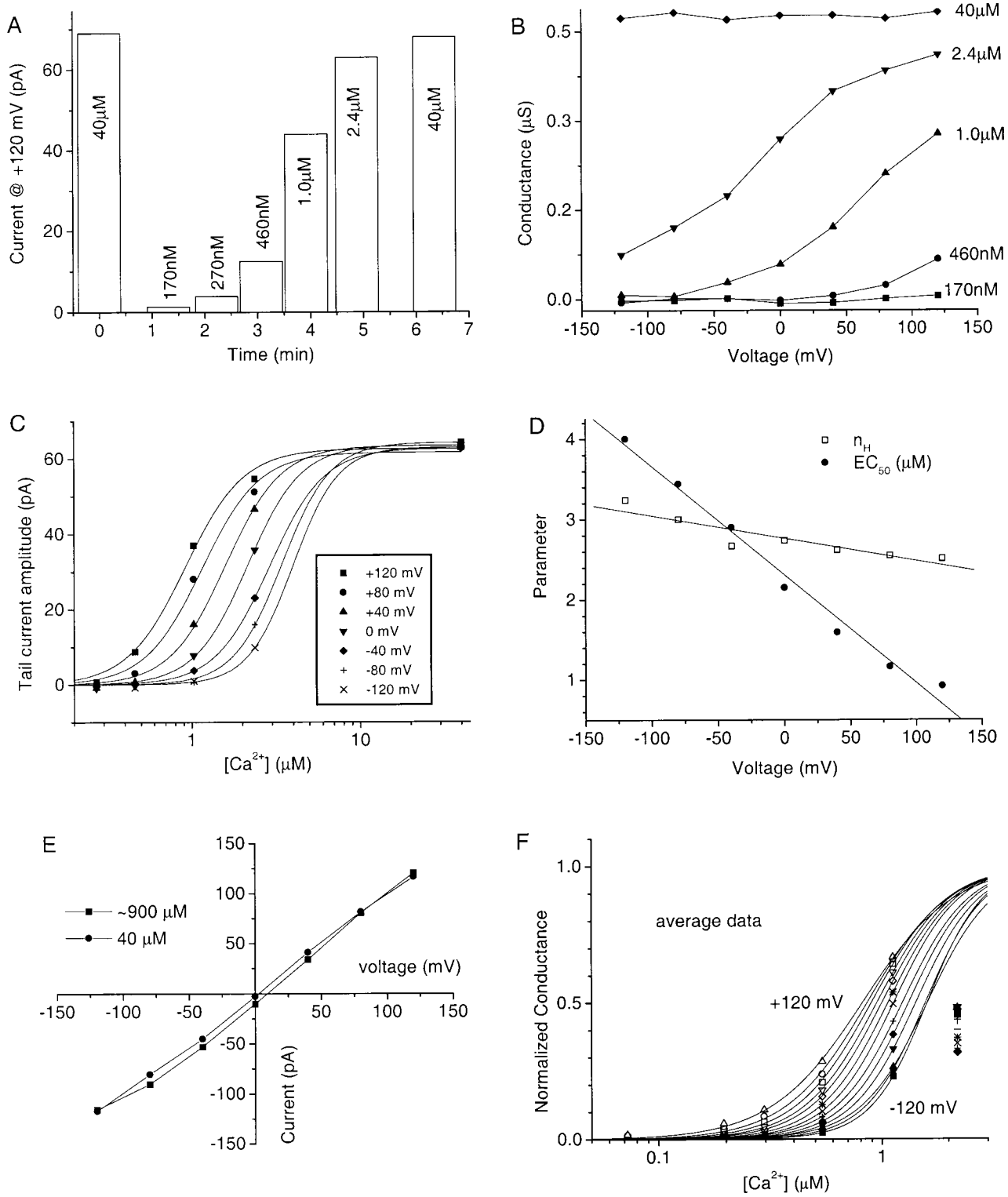

Figure 6. Voltage-dependent Ca^{2+} affinity of Ca^{2+}-activated Cl channels. (A) Time course of current rundown in a champion patch. The amplitude of currents at +120 mV in the presence of different $[Ca^{2+}]$ are plotted with time after patch excision. The patch was exposed to Ca^{2+} only during the voltage-clamp episodes. (B) Voltage-dependent conductance of the champion patch. The experiment was performed as described in Fig. 4 A. (C) Voltage dependence of Ca^{2+} affinity of champion patch. The tail current amplitudes used to create the plot in B were replotted as a function of $[Ca^{2+}]$ and fitted to the Hill equation. (D) The best-fit parameters of the data in C to the Hill equation. (E) Demonstration that 40 μM Ca^{2+} produces a maximal Cl current. Steady state I-V curves are shown for Ca^{2+}-dependent currents in 40 μM (●) and ~900 μM (■) Ca^{2+}. (F) Average apparent affinity of the channel for Ca^{2+} at different voltages. Normalized conductance from Fig. 4 A was replotted as a function of $[Ca^{2+}]$. Error bars are not shown for clarity but can be obtained from Fig. 4. The data for $[Ca^{2+}] < 2$ μM were fitted to the Hill equation.

In this scheme, channel opening is controlled by Ca^{2+} binding to more than one site in a voltage-independent manner. The voltage dependence of the currents is proposed to be due to the voltage dependence of the closing rate constants β (V). At low [Ca^{2+}], where channel opening rate is slow, the current outwardly rectifies and exhibits time-dependent activation and deactivation, because hyperpolarization accelerates channel closure and shifts the equilibrium from the open to the closed states. In contrast, at high [Ca^{2+}], the channel opening rate is rapid and there are multiple paths for channel opening because channels have more than one Ca^{2+} bound. Consequently, voltage-dependent changes in the closing rate will have less effect on the macroscopic currents. This scheme also explains why channels cannot be opened by depolarization in the absence of Ca^{2+} or why they cannot be closed by voltage in the presence of Ca^{2+}.

Voltage Dependence of Current Activation and Deactivation

To test this model further, we examined in detail the kinetics of current activation and deactivation at different [Ca^{2+}]. The deactivation was determined by exponential fitting of the tail current decay at various potentials after a depolarizing step to +120 mV (Fig. 7). At all [Ca^{2+}] examined, the deactivating tail currents observed upon repolarization to different potentials from +120 mV were well fitted by single exponentials (superimposed, but hard to discern in Fig. 7). τ_{deact} increased with depolarization and increased with increasing [Ca^{2+}] within the submicromolar range (Fig. 8 A). The equivalent off gating charge movement, calculated by fitting plots of τ_{deact} vs. V_m to the equation $\tau_{deact} = Ae^{qFV/RT} + b$, was 0.35 at 280 nM Ca^{2+}, 0.27 at 460 nM, 0.26 at 680 nM, and 0.12 at 1 μM Ca^{2+} (Fig. 8 B). These data are consistent with a model in which there was a dominant rate-limiting transition in the backward direction from the open to the closed states, which was voltage sensitive at low [Ca^{2+}]. At higher [Ca^{2+}], the voltage sensitivity became less and deactivation was incomplete because the forward voltage-independent reaction shifted the equilibrium strongly towards open states, regardless of the backward voltage-dependent reaction.

We then examined the kinetics of current activation. Depolarizing steps elicited outward currents that exhibited a small instantaneous component followed by a slow activation that took ~1 s to reach maximum (Fig. 9). Activation of the currents could be fitted with single exponentials, but the fits were often disappointing. Specifically, using least squares algorithms, if the rising phase of the current was well fit, the plateau was usually poorly fit. Using the Pade-LaPlace method (Yeramian and Claverie, 1987; Bajzer et al., 1989) for fitting curves to sums of exponentials without a hypothesis about the number of components, one fast exponential component plus another slower nonexponential component were found. Regardless of the method used for fitting the activation, the time constants of the exponential components of the activation usually were weakly influenced by membrane potential or increased with depolarization (Figs. 9 and 10 A). If channel opening were voltage sensitive, we would expect channel activation to accelerate with depolarization. Although activation was not clearly voltage dependent, activation was Ca^{2+} dependent: activation became faster with increasing [Ca^{2+}] (Fig. 10 B). We interpret the increased current produced by depolarization at low [Ca^{2+}] as a consequence of a shift in the equilibrium between closed and open states as a result of changing the voltage-sensitive backward rate constant β. The time constant of the approach to the new equilibrium upon depolarization will approximate $1/(\alpha\ [Ca^{2+}] + \beta)$. Thus, as β becomes larger with hyperpolarization, the time constant of activation will become smaller for a constant α [Ca^{2+}]. This is observed with the lowest [Ca^{2+}] in Fig. 10 A. With higher [Ca^{2+}], α [Ca^{2+}] dominates the reaction and the effect of changing β is negligible. As the [Ca^{2+}] becomes greater, the time constant of activation becomes smaller, as expected from the model.

Current Activation and Deactivation in Response to Rapid Ca^{2+} Applications

As another test of this model, we examined the response of the current to rapid applications of Ca^{2+} at constant transmembrane potentials. The solution bathing the cytosolic face of the patch was changed from <10 nM Ca^2 to various [Ca^{2+}] in <3 ms (Fig. 11 A) as described in METHODS. The membrane potential was held at voltages between −120 and +120 mV and the Ca^{2+} concentration was jumped for a 5-s duration (Fig. 11 B). The turn-on and -off of the current with rapid Ca^{2+} perfusion were characterized by time constants, called τ_{on} and τ_{off} to distinguish them from voltage-dependent activation τ_{act} and τ_{deact} described in Figs. 7–10. At 40 μM Ca^{2+}, the current increased very rapidly (with a τ_{on} that was probably limited by the switching time of the solution) at all potentials (Fig. 11, C and E). The τ_{off} upon washing out Ca^{2+} was voltage dependent and was fit by a single exponential. The current turned off more slowly at more positive potentials (Fig. 11, C and D). In a different patch, when the solution was switched from <10 nM Ca^{2+} to 400 nM Ca^{2+}, τ_{on} was much slower (Fig. 11, F and H), but τ_{off} was very similar to that observed at 40 μM Ca^{2+} (F and G).

The mean data from many such experiments are shown in Fig. 12. Although there was some variability among experiments, τ_{off} was independent of Ca^{2+} and was an exponential function of voltage, being greatest at depolarized potentials (Fig. 12 A). The plot of τ_{off} versus voltage was quantitatively similar to the plot of

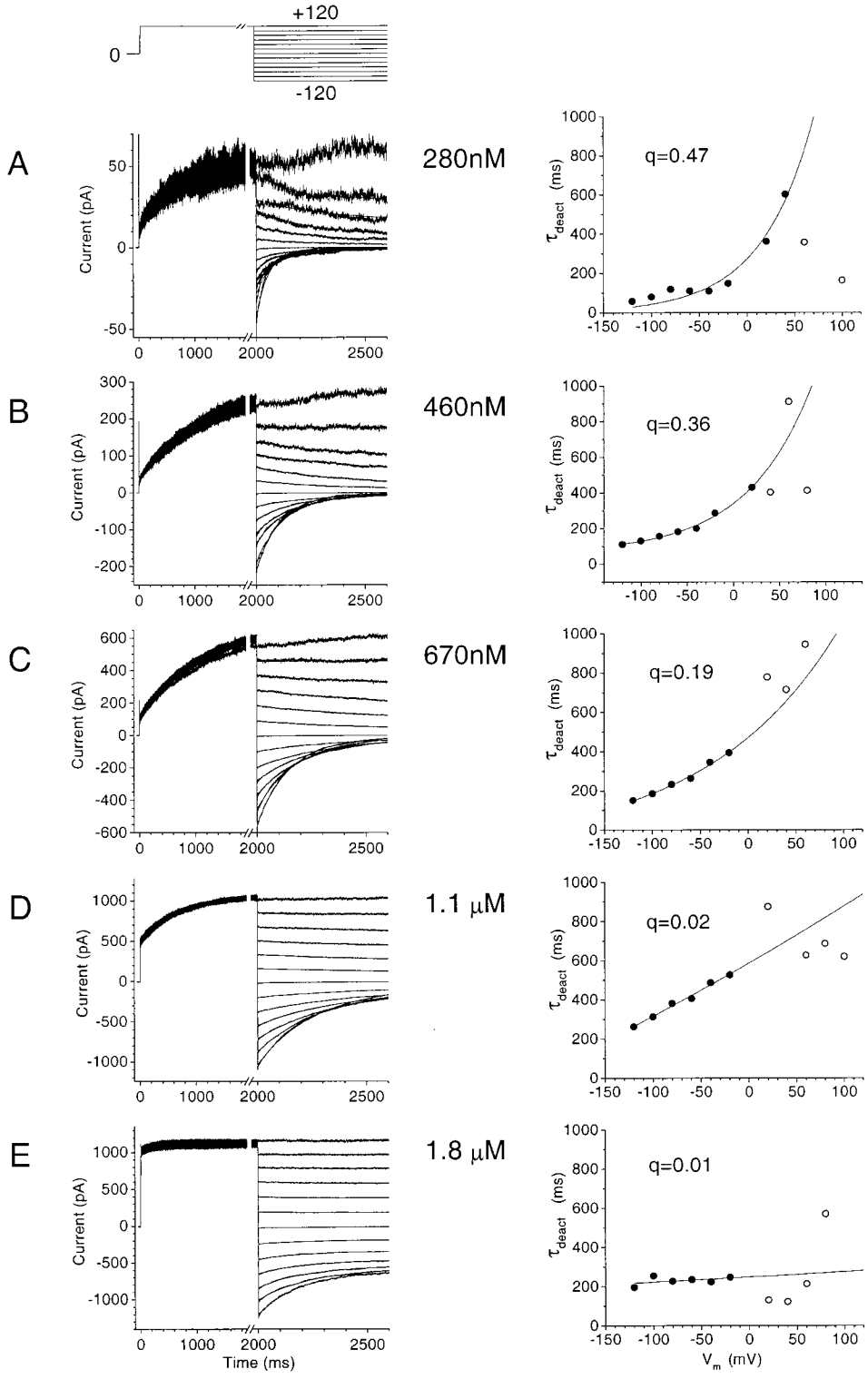

Figure 7. Kinetic analysis of deactivation of Ca^{2+}-activated Cl^- currents in a representative excised patch. Currents were elicited by voltage-clamp steps applied while the cytosolic face of the patch was bathed in solutions with different free $[Ca^{2+}]$: (A) 280 nM Ca^{2+}, (B) 460 nM Ca^{2+}, (C) 670 nM Ca^{2+}, (D) 1.1 μM Ca^{2+}, and (E) 1.8 μM Ca^{2+}. The patch was voltage clamped by depolarizing to +120 mV, and then stepping to various potentials between +120 and −120 mV. The tail currents were fitted to single exponentials (superimposed) and the time constants were plotted versus membrane potential. Solid curves in the right panels are best fits of the solid symbols to the equation $\tau_{deact} = Ae^{qFV/RT} + b$.

τ_{deact} versus voltage (Fig. 8 A) for low $[Ca^{2+}]$. The value of q estimated from Fig. 12 A was 0.26. Both the data from voltage jumps and Ca^{2+} concentration jumps are consistent with deactivation of the current being dominated by a single voltage-dependent step.

In contrast to the Ca independence of τ_{off}, τ_{on} was strongly dependent on $[Ca^{2+}]$: activation was faster at higher $[Ca^{2+}]$ (Fig. 12 B). τ_{on} was voltage independent at high $[Ca^{2+}]$, but became progressively more voltage dependent as $[Ca^{2+}]$ was lowered. Because τ_{on} for a simple two-state model will be equal to $1/\alpha + \beta$ (where α is the forward and β is the backward rate constant),

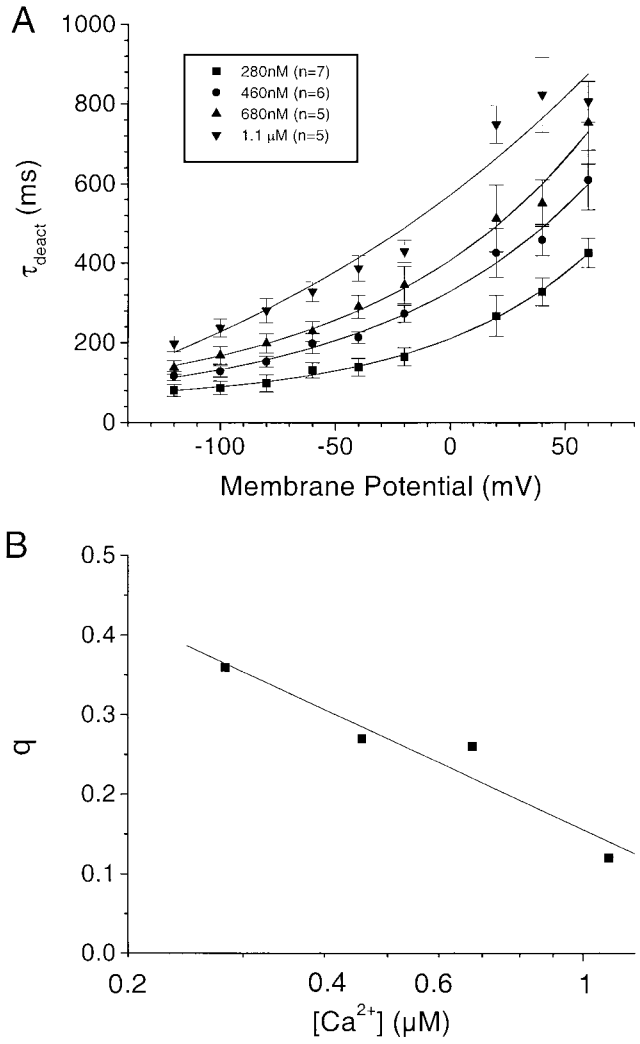

Figure 8. Average data for deactivation of Ca^{2+}-activated Cl^- currents. The experiments were performed as in Fig. 7. (A) The data were averaged for 280 nM Ca^{2+} ($n = 7$), 460 nM Ca^{2+} ($n = 6$), 680 nM Ca^{2+} ($n = 5$), and 1.1 μM Ca^{2+} ($n = 5$). The data were fitted to the equation $\tau_{deact} = Ae^{qFV/RT} + b$. (B) The q values calculated from the fits in A were plotted vs. $[Ca^{2+}]$.

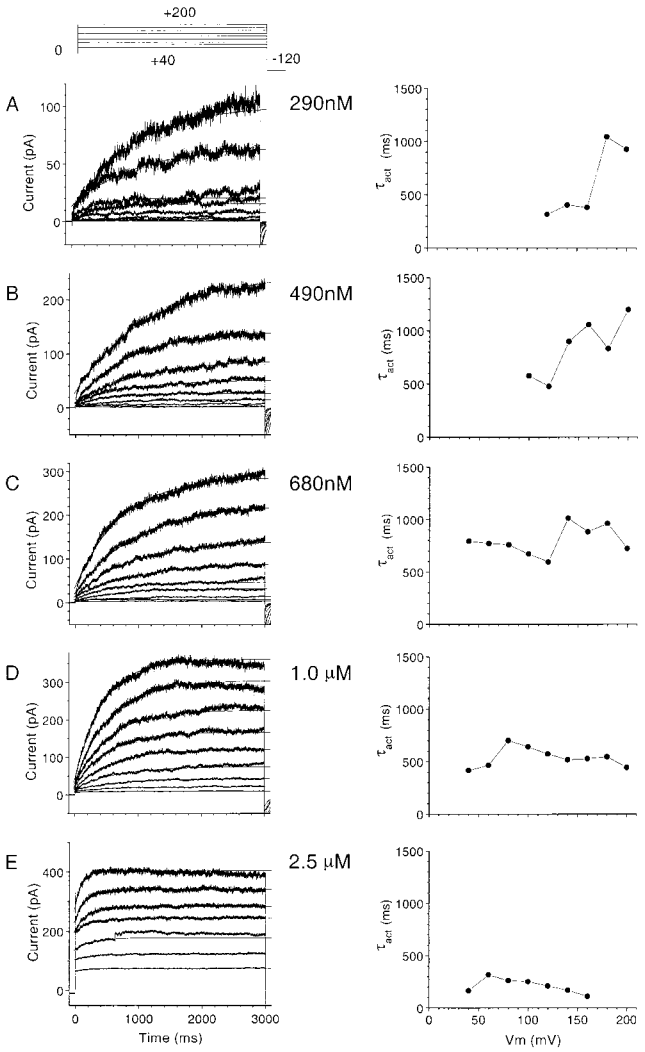

Figure 9. Kinetic analysis of activation of Ca^{2+}-activated Cl^- currents in a representative excised patch. Currents were elicited by voltage-clamp steps applied while the cytosolic face of the patch was exposed to solutions with different free $[Ca^{2+}]$. The patch was voltage clamped by stepping to various potentials between +200 and +40 mV. The activating phase of the currents were fitted to single exponentials (superimposed) and the time constants were plotted versus membrane potential.

as α becomes slower at low $[Ca^{2+}]$, τ_{on} will approach $1/\beta$. Thus, the apparent voltage dependence of τ_{on} at low $[Ca^{2+}]$ can be explained by the voltage dependence of the backward reaction.

Ionic Selectivity of the Channel

Using two-microelectrode voltage clamp, we have previously shown that both inward (I_{Cl2}) and outward ($I_{Cl1\text{-}S}$ and $I_{Cl1\text{-}T}$) Ca^{2+}-activated Cl^- currents have the same anionic selectivity sequence ($I^- > Br^- > Cl^-$), which is consistent with sequence 1 of Eisenman (Wright and Diamond, 1977). But there were quantitative differences between these three currents (Kuruma and Hartzell, 1999). Although we questioned whether these differences might be explained by technical artifacts, we also raised the possibility that inward and outward currents might be carried by different species of channels. To examine this idea further, we measured the anionic selectivity of the inward and outward currents in different $[Ca^{2+}]$ in excised patches using the same voltage protocols we used in our two-microelectrode voltage-clamp study (Kuruma and Hartzell, 1999).

Cytosolic Cl^- was partially replaced with I^- or Br^- and the change in reversal potential of the instantaneous tail currents was measured. Fig. 13 shows the ef-

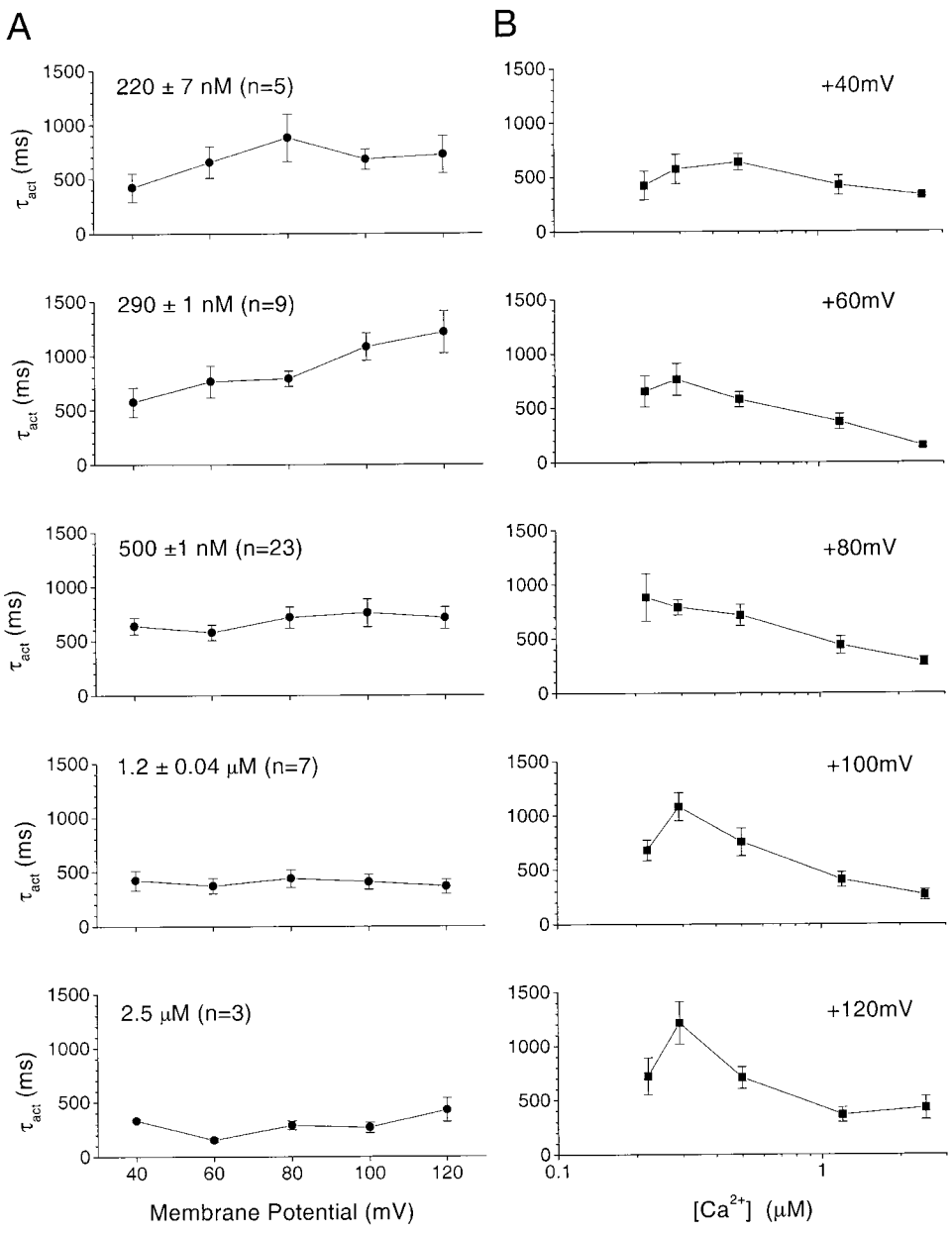

Figure 10. Average data for activation of Ca^{2+}-activated Cl^- currents in excised patch. The experiments were performed as in Fig. 9. (A) Dependence of current activation on voltage at different $[Ca^{2+}]$. (B) The data from A were replotted to show the dependence of current activation on free $[Ca^{2+}]$.

fects of changing from Cl^- to I^--containing solutions with three different conditions: (a) outward current at low $[Ca^{2+}]$ (1 μM), where outward current shows time-dependent activation (mimicking $I_{Cl1\text{-}S}$) and inward current is small (Fig. 13, A–C); (b) outward current at high $[Ca^{2+}]$ (2 μM), where both outward and inward currents were fully developed (Fig. 13, D–F); and (c) inward current under the same condition as b (Fig. 13, G–I). We measured the shift in reversal potentials and the calculated permeability ratio using Goldman-Hodgkin-Katz equation (Hille, 1992). As shown in Fig. 13 J, the anionic selectivity with the three different conditions was quantitatively identical to a relative anionic selectivity of I > Br > Cl 3.6:1.9:1.0. On this basis, we can exclude the hypothesis that there are two types of channels with different anionic selectivities.

Modeling the Experimental Data

To test whether the gating scheme proposed above could describe the kinetics of the Ca-activated Cl currents, we calculated the expected macroscopic currents using this gating scheme and the rate constants derived from our experiments.

We first calculated the currents activated by rapid Ca^{2+} application as in Fig. 11. We assumed three Ca^{2+}-liganded states with identical and independent affinities for Ca^{2+}. The Ca^{2+}-dependent on rate per binding

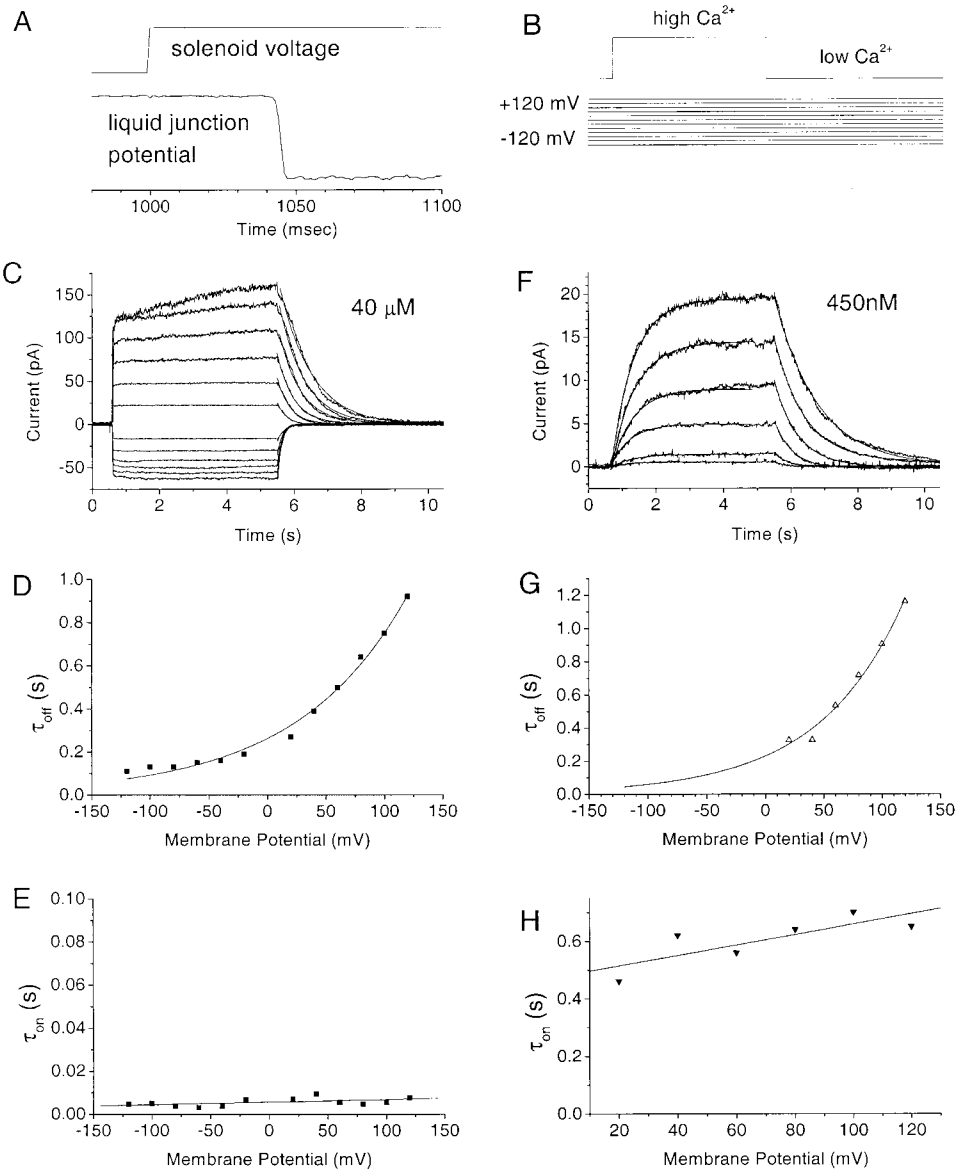

Figure 11. Activation of Ca^{2+}-activated Cl^- currents in an excised patch by rapid perfusion of Ca^{2+}. (A) Calibration of rate of change of solution. The liquid junction potential of a high resistance (50 MΩ) electrode placed in the solution stream was measured as the solution was changed from 0.1 to 2 M KCl. (Top) Solenoid voltage, (bottom) liquid junction potential. There is an ~40-ms lag between switching the solenoid and the onset of the change in junction potential due to the dead volume of the perfusion line. Once the potential begins to change, the time to change from 10 to 90% of maximum was ~3 ms. (B) Protocol. The patch was switched to a voltage between +120 and −120 mV from the holding potential of 0 mV, 5 s before changing the perfusion from low to high $[Ca^{2+}]$. (C) Current traces recorded upon switching from <10 nM Ca^{2+} to 40 μM Ca^{2+} (the activation and deactivation are fitted to single exponentials; superimposed). (D) The time constant of turn off (τ_{off}) of the current was plotted versus potential. (E) The time constant of the turn on (τ_{on}) of the current was plotted versus potential. (F) Current traces recorded upon switching from <10 to 450 nM Ca^{2+}. Single exponential fits to activation and deactivation are superimposed. (G and H) Time constants as a function of potential.

site was assumed to be 3×10^6 mol^{-1} s^{-1} and the Ca^{2+}-independent off rate was assumed to be 50 s^{-1}. The rate constants α_1, α_2, and α_3 for conversion from closed states to open states were assumed to be Ca^{2+} and voltage independent and were assumed to be more rapid as the closed states became more heavily Ca^{2+} liganded ($\alpha_1 = 10$, $\alpha_2 = 30$, $\alpha_3 = 100$). The backward rates from open to closed were assumed to be voltage dependent according to the equation $\beta(V) = k * \exp(V_1 + V_m * V_2)$. k, V_1, and V_2 were estimated by fitting the off rates derived from the data in Fig. 12 A to the equation. The values were $k = 224$, $V_1 = -3.8$, and $V_2 = -10$. For simplicity, we ignored transitions between open states.

Fig. 14 shows simulations of the macroscopic currents using a Monte-Carlo modeling program developed by Dr. Steve Traynelis (Emory University School of Medicine). The currents in response to Ca^{2+} jumps from <10 nM to 50 μM Ca^{2+} (Fig. 14 A) and 500 nM Ca^{2+} (Fig. 14 B) closely approximate the experimentally recorded currents in both waveform and rectification (compare with Fig. 11, C and D). The τ_{off} and τ_{on} of the simulated and actual currents are similar (compare Fig. 15, E and F, with 11, D–H). The model also predicts well the currents observed in response to voltage-clamp steps (Fig. 14, C and D). Simulated currents in excised patches in response to voltage pulses at 50 μM Ca^{2+} (Fig. 14 C) and 500 nM Ca^{2+} (D) also approximate the behavior of the actual currents (compare with Fig. 3). Also, the current–voltage relationship shifts from outwardly rectifying to linear within this range of $[Ca^{2+}]$ (Fig. 14 G), as was described in Fig. 3.

The model is a reasonable approximation to the data,

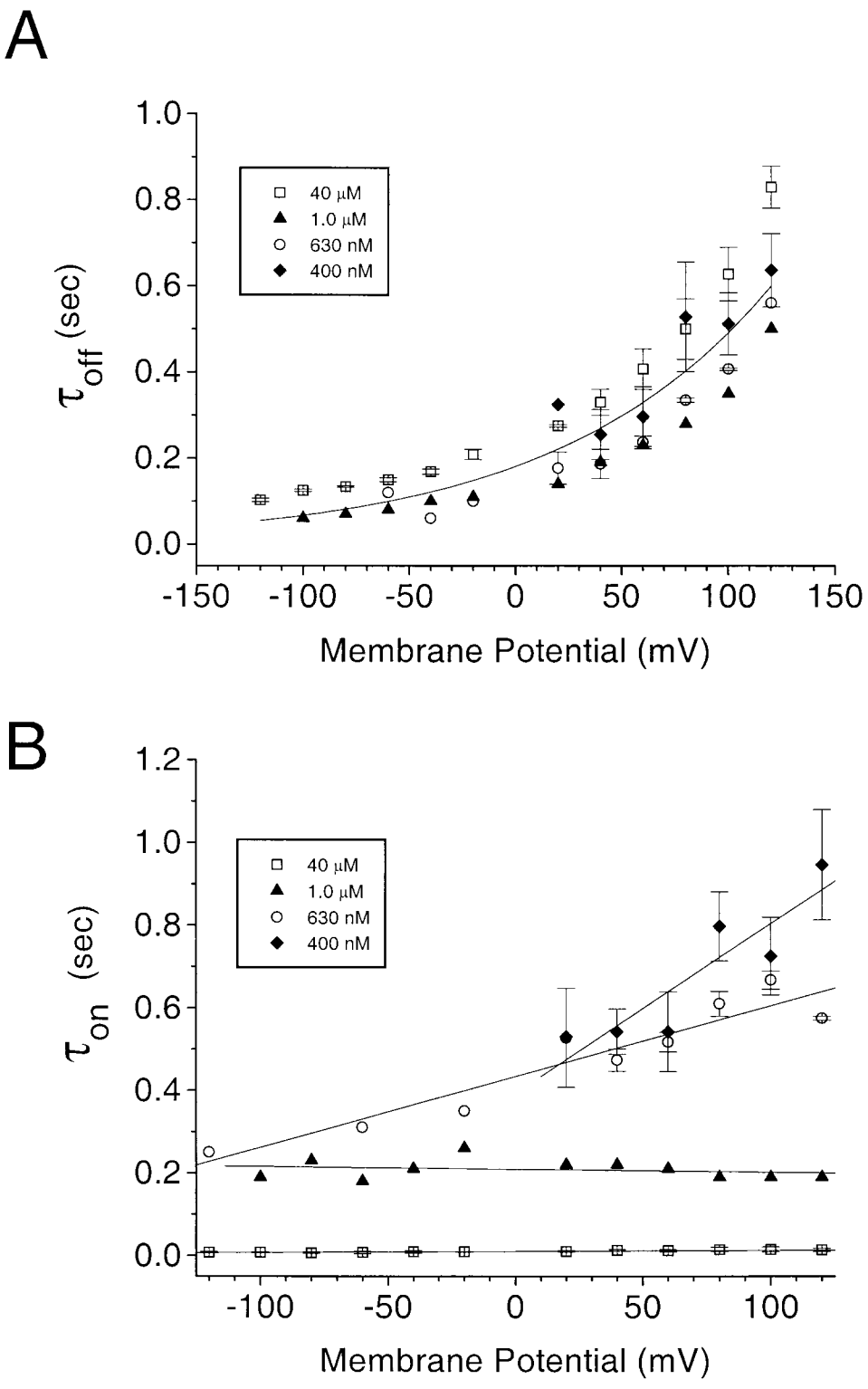

Figure 12. Average data (n = 3–15) from rapid perfusion experiments. Experiments were performed as described in Fig. 11. τ_{off} (A) and τ_{on} (B) are plotted for 40 μM Ca^{2+} (□), 1 μM Ca^{2+} (▲), 630 nM Ca^{2+} (○), 400 nM Ca^{2+} (◆). The solid line in A is a single exponential fit to the average of all the data at different [Ca^{2+}]: τ_{off} = 0.064 * exp (0.26 * FV/RT).

but it fails quantitatively to predict the time course of current deactivation in response to voltage pulses from positive potentials to −120 mV at steady 500 nM Ca^{2+} (Fig. 14 E). The kinetics of simulated current deactivation were slower than we observed experimentally. Also, the model predicts that τ_{off} is somewhat slower for 50 μM Ca^{2+} than for 500 nM Ca^{2+}, which was not observed experimentally. Manipulation of the various rate constants were not able to correct these differences without introducing other discrepancies between the data and the

model. Thus, although this gating scheme simulates the general features of the data, it is only a rough approximation. It is possible that rundown may contribute to the differences between the model and the data.

It was not possible to model the data with schemes in which the forward opening rate constants were voltage sensitive. It was possible to reproduce some of the general features of the actual currents with schemes having fewer states. A simple two-step closed–open reaction with the forward rate being Ca^{2+} sensitive and the backward rate being voltage sensitive was able to roughly model the currents, but the quantitative correspondence with the data was not as good as the multistate model presented here.

Cl Currents Can Be Excitatory or Inhibitory, Depending on the Ca^{2+} Signals

The data in this paper show that, depending on the level of cytosolic Ca^{2+}, a single species of Cl channel can behave qualitatively differently. This could be important in excitable cells where, at low [Ca^{2+}], these channels would carry mainly outward current and thus come into play in repolarizing the cell after an excitatory stimulus. In contrast, at high [Ca^{2+}], these channels could also carry inward current at resting potentials below E_{Cl} (between −30 and −60 mV in most excitable cells) and become excitatory. We tested this hypothesis in the oocyte model by examining the ability of IP_3-stimulated Ca^{2+} release from stores and Ca^{2+} influx to regulate the Cl^- currents (Fig. 15). Ca^{2+} influx was controlled by the heterologously expressed ligand-gated inotropic glutamate receptor ($iGluR_3$) that was activated by application of kainic acid under conditions where the only permeant cation present was Ca^{2+}. In the absence of activation of $iGluR_3$, injection of IP_3 stimulated Ca^{2+} release from stores and activation of outward current at +40 mV (Fig. 15, A and B). The inward current observed under these conditions was due to slow deactivation of the tail current (Fig. 15 B): very little steady state inward current was detectable. However, if $iGluR_3$ was activated with kainic acid to induce a small amount of Ca^{2+} influx, injection of the same amount of IP_3 now resulted in a large increase in both inward and outward currents (Fig. 15 C). Cytosolic Ca^{2+} was measured in the same oocyte simultaneously by confocal microscopy during the +40 and −120 mV voltage-clamp pulses (Machaca and Hartzell, 1999) (Fig. 15 E). Application of kainic acid caused a small influx of Ca^{2+}, detected as a voltage-dependent increase in fluorescence at −120 mV (larger at −120 mV where the driving force for Ca^{2+} influx was high). Injection of IP_3 then stimulated a voltage-independent release of Ca^{2+} from stores. The small increase in Ca^{2+} influx after the peak Ca^{2+} signal was due to development of store-operated Ca^{2+} influx (Machaca and Hartzell, 1999). These data show that altering the basal cytosolic [Ca^{2+}] within a range that has little direct effect on the Ca^{2+}-activated Cl^- channels can strongly modulate the current produced by a larger Ca^{2+} signal and switch the Cl^- current from outward only to both inward and outward. Thus, depending on the membrane potential and E_{Cl} (which may be modulated by other Cl^- channels and transporters), the amplitude of the Ca^{2+} signal can result in an excitatory or inhibitory response mediated by the same ion channel.

DISCUSSION

Gating Mechanisms of Ca^{2+}-activated Cl^- Channels

The data presented here are consistent with the gating scheme proposed in RESULTS in which Ca^{2+}-activated Cl^- channels exist in multiple closed states having zero to three Ca^{2+} ions bound. This is supported by the data in Fig. 6 showing that the relationships between conductance and Ca^{2+} are fitted by curves with Hill coefficients between 2.5 and 3.2. The channel cannot open from the Ca^{2+}-free state (C_0), because potentials as large as +200 mV do not activate current at <10 nM Ca^{2+} (Figs. 1 and 3). However, it is likely that the channel can open from each of the Ca-liganded closed states ($C_1 \sim C_n$). The transition from the closed to open states is virtually voltage independent, as shown by the voltage independence of activation (Figs. 10 and 12 B). However, the transition from open to closed is voltage sensitive because the deactivation of the current by voltage or Ca^{2+} concentration jumps is fit by a single exponential and is voltage dependent (Figs. 8 and 12). The leftward shift of the conductance–voltage curve with increasing [Ca^{2+}] is explained by the fact that as more channels bind Ca^{2+}, the overall equilibrium is shifted towards open channels. At hyperpolarized potentials, the equilibrium can be shifted towards closed states by increasing the rate constant for channel closing. However, at high [Ca^{2+}], β is slow relative to the opening rates so that voltage has little effect under these conditions.

This gating scheme is supported by data from other laboratories. Gomez-Hernandez et al. (1997), using excised patches from *Xenopus* oocytes, showed that activation of the current by Ca^{2+} concentration jumps at high [Ca^{2+}] (1.8 mM and 27 μM) was voltage independent, whereas deactivation was voltage dependent, as we show in Fig. 12 A. But these authors did not examine the kinetics of currents exposed to lower [Ca^{2+}]. Our data also complement whole-cell data from other laboratories on rat parotid gland cells (Arreola et al., 1996) and microvascular endothelial cells (Nilius et al., 1997b). Both of these laboratories perfused intact cells with solutions containing different [Ca^{2+}] in the whole-cell mode and showed that the channels in these cells were regulated by both Ca^{2+} and voltage. Our data differs from theirs in one respect. They find that the Hill

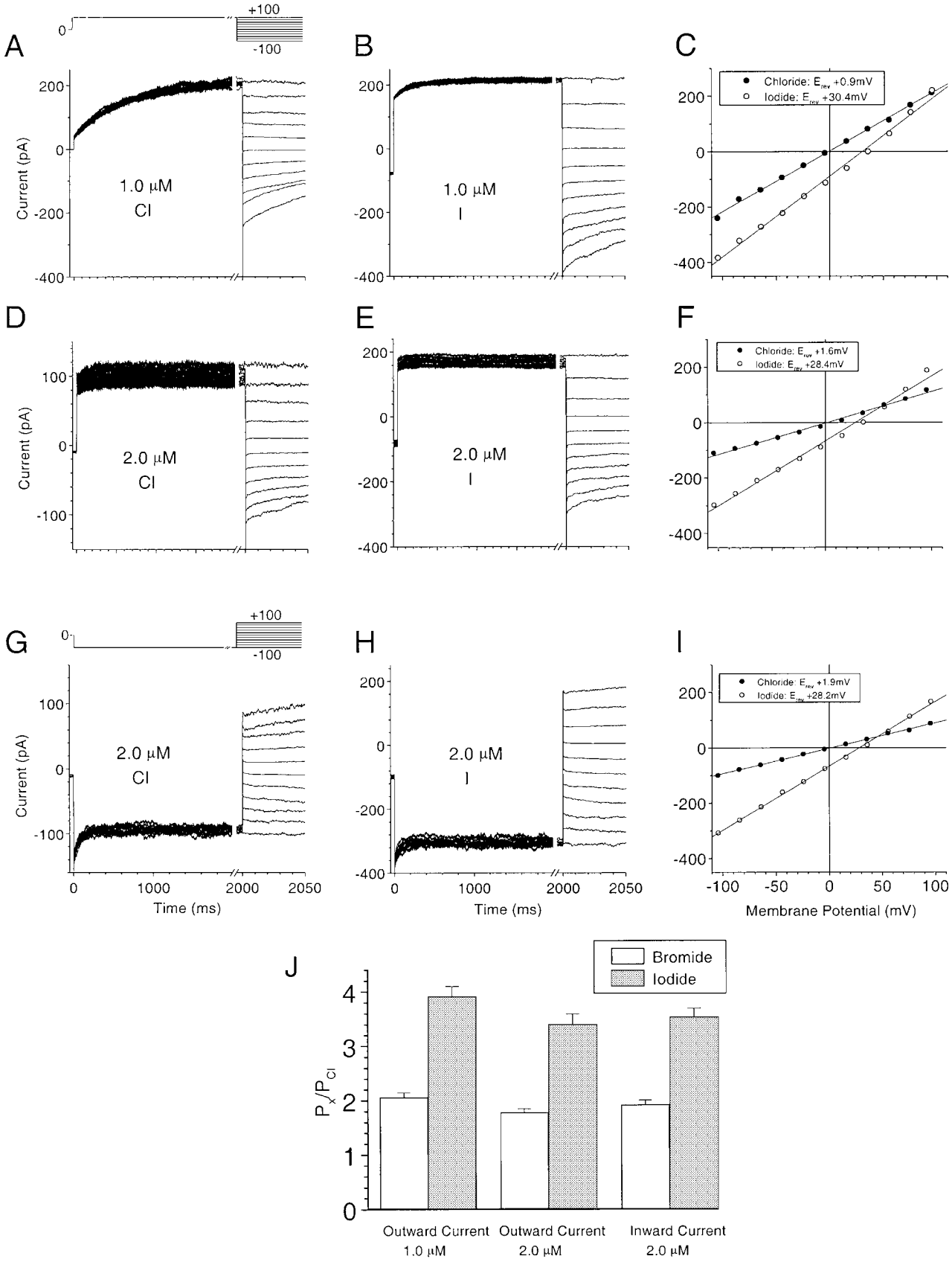

Figure 13. Anionic selectivity of the channel. The reversal potential of the outward currents activated by 1 (A–C) and 2 (D–F) μM Ca^{2+} were determined by measuring the instantaneous tail currents at different potentials following a pulse to +100 mV. The voltage protocol is

coefficient increases with depolarization, but we find that it decreases slightly.

It is interesting to compare this kinetic scheme with one proposed by Cui et al. (1997) for the large-conductance Ca^{2+}-activated K (BK) channel. There are several fundamental differences between BK channel gating and our gating model of the Ca^{2+}-activated Cl^- channel. First, the BK channel exhibits intrinsic voltage dependence and can be opened by voltage in the absence of Ca^{2+} or closed by voltage in the presence of Ca^{2+}. This is not true of the Ca^{2+}-activated Cl^- channel because the opening rate constant is not voltage sensitive. Because the voltage dependence of the Ca^{2+}-activated Cl^- channel results from the voltage dependence of the closing rate, the channel obviously cannot be opened in the absence of Ca^{2+} by altering the closing rate constant. Likewise, in the presence of Ca^{2+}, there will always be an equilibrium level of open states, regardless of the value of $\beta(V)$. Thus, voltage will not be capable of completely turning off the current.

Mechanisms of Regulation of Ca^{2+}-activated Cl^- Channels

There remains considerable uncertainty about whether Ca^{2+}-activated Cl^- channels are activated by direct binding of Ca^{2+}, by binding of calmodulin (CaM)[1] or other Ca^{2+}-binding proteins, or by Ca^{2+}-dependent enzymatic modification (phosphorylation/dephosphorylation). Some channels can be stably activated in excised patches by Ca^{2+} in the absence of ATP (Frizzell et al., 1986; Takahashi et al., 1987; Martin, 1993; Collier et al., 1996; Gomez-Hernandez et al., 1997), suggesting that channels might be regulated directly by Ca^{2+} binding to the channel. In other experiments, however, channel activity runs down quickly after excision, suggesting the possibility that components in addition to Ca^{2+} are required to open the channel (Klöckner, 1993; Morris and Frizzell, 1993; VanRenterghem and Lazdunski, 1993; Large and Wang, 1996; Schlenker and Fitz, 1996; Nilius et al., 1997a). In our experiments, the currents often ran down, in contrast to what has been reported by some other labs on the same preparation (Gomez-Hernandez et al., 1997; Takahashi et al., 1987). However, the possibility exists that in the experiments of these other labs, rundown had already occurred before recording began.

It has been shown that some types of Ca^{2+}-activated Cl currents require Ca^{2+}-dependent phosphorylation for activation. A role for CaMKII-dependent phosphorylation in the activation of certain Ca^{2+} activated Cl^- currents has been suggested because the currents are inhibited by KN62 or a CaMKII-inhibitor peptide (Nishimoto et al., 1991; Tohda et al., 1991; Wagner et al., 1991; Worrell and Frizzell, 1991; Morris and Frizzell, 1993; Schumann et al., 1993; Chan et al., 1994; Braun and Schulman, 1995; Chao et al., 1995; Xie et al., 1996; Arreola et al., 1998). CaMKII, however, is apparently not required for activation of all kinds of Ca^{2+}-activated Cl channels: a recent study showed that, although macroscopic currents in parotid gland and T84 intestinal cells are very similar, the currents in T84 cells are inhibited by CaMKII inhibitors, whereas the currents in parotid cells are not (Arreola et al., 1998). These differences could possibly be explained by differences in the activity of protein phosphatases in the different cell types or to differences in the regulation of different kinds of Ca^{2+}-activated Cl channels. To make the situation more complicated, in smooth muscle cells, CaMKII-dependent phosphorylation inhibits channel activity (Wang and Kotlikoff, 1997) and in A6 kidney cells alkaline phosphatase (presumably via protein dephosphorylation) increases inward currents (Marunaka and Eaton, 1990).

The experiments we present here show clearly that the channel can be activated by Ca^{2+} in the absence of ATP and thus show that the transition from the closed to the open state is not tightly coupled to phosphorylation and is probably due to direct Ca^{2+} binding to a channel subunit. The rundown phenomenon, however, could be due to dephosphorylation of channels that are phosphorylated before the patch is excised, but if this is the case, phosphorylation would only make the channel competent to be opened by Ca^{2+} and would not open the channel directly.

Physiological Significance

Ca^{2+}-activated Cl^- channels are certainly less well understood than cation channels or some other anion channels, such as CFTR, γ-aminobutyric acid receptors, or the ClC family (Jentsh and Gunther, 1997). Nevertheless, it is clear that these channels are found in many cell types and play important roles in many tissues, including smooth muscle and epithelia (Large and Wang, 1996; Morris, 1999).

These data have a number of important physiological implications. In *Xenopus* egg, sperm entry during fertilization turns on Ca^{2+}-activated Cl^- channels as a conse-

[1]*Abbreviations used in this paper:* CaM, calmodulin; $iGluR_3$, inotropic glutamate receptor.

shown above A. The reversal potential of the inward currents activated by 2 μM Ca^{2+} (G–I) were determined in the same way following a pulse to −100 mV. The voltage protocol is shown above G. The pipet solution contained 158.4 mM Cl^-, the bath contained either 158.4 mM Cl^- (A, D, and G) or 150 mM I^- and 8.4 mM Cl^- (B, E, and H). (C, F, and I) Tail current amplitudes for the symmetrical chloride solutions (●) and the low Cl^-, high iodide solution (○). (J) Bar graph of the anionic permeability ratios (P_x/P_{Cl}) for outward currents at 1 and 2 μM Ca^{2+} and for inward current at 2 μM Ca^{2+}.

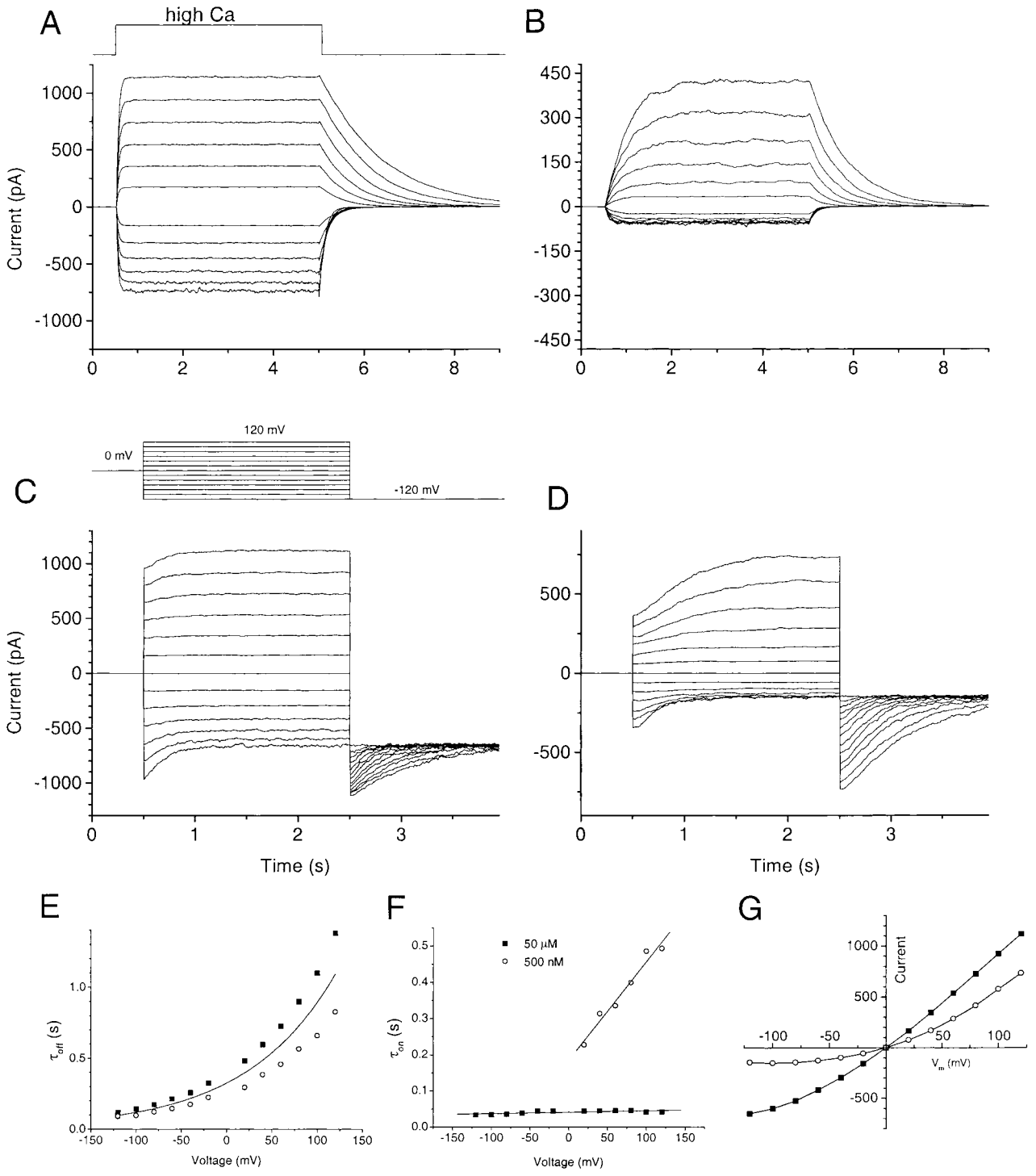

Figure 14. Simulation of Ca^{2+}-activated Cl currents using the model and rate constants described in the text. The macroscopic currents were modeled using a Monte-Carlo simulation program written by Dr. Steve Traynelis. (A and B) Simulated currents in response to Ca^{2+} steps from <10 nM to 50 μM (A) or 500 nM (B). (C and D) Simulated currents in response to voltage-clamp pulses from 0 mV to voltages between +120 and −120 mV (20-mV increments) at a steady 50 μM Ca^{2+} (C) or 500 nM Ca^{2+} (D). (E) Deactivation time constants measured from traces in A and B. (F) Activation time constants measured from simulated currents in A and B. (G) Steady state current–voltage relationship for simulated currents in C and D.

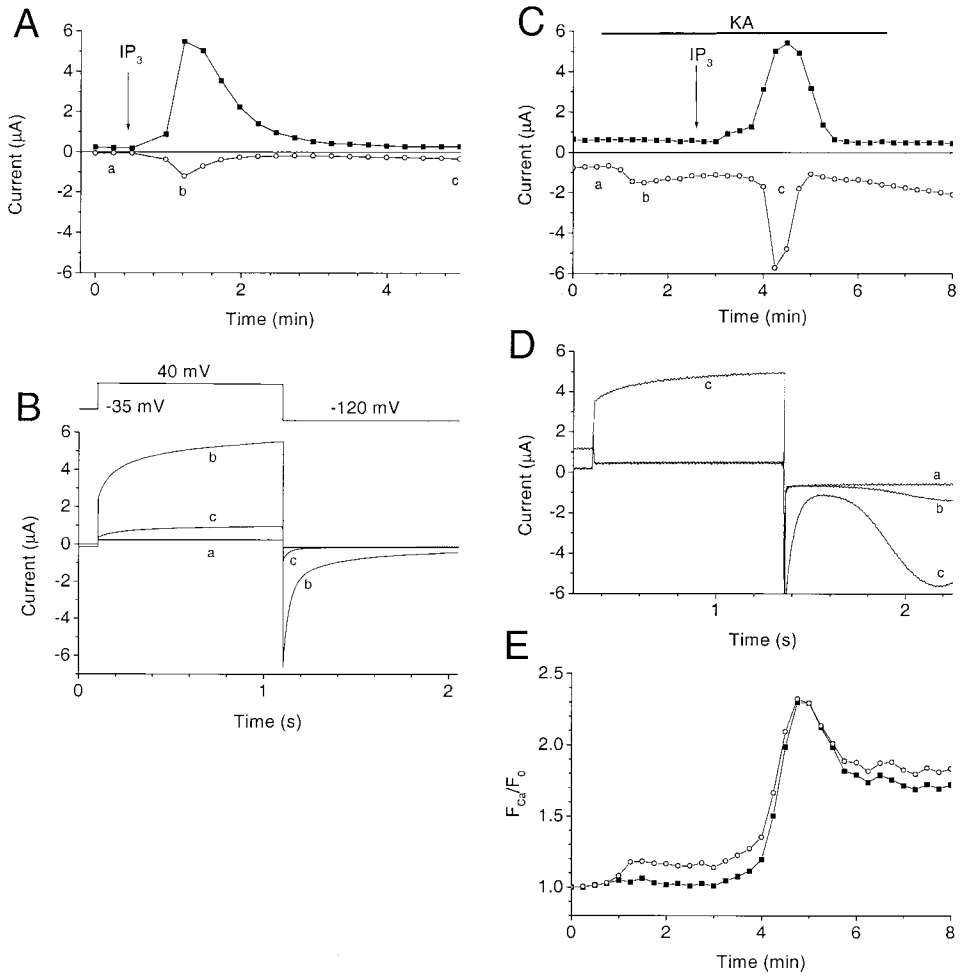

Figure 15. Ca^{2+} concentration determines direction of Cl current in intact cells. Normal oocytes (A and B) or oocytes heterologously expressing $iGluR_3$ (C–E) were bathed in normal Ringer solution (A and B) or NMDG-Ringer (C–E) and were voltage clamped with two microelectrodes, injected with 23 nl 1 mM IP_3 (arrows), and exposed to 100 μM kainic acid (KA) in the bath as indicated (bar) (Kuruma and Hartzell, 1999). The voltage protocol was an ~1-s duration pulse to +40 mV, followed by an ~1-s pulse to −120 mV from a holding potential of −35 mV. (A and C) Plot of current amplitudes during the experiment. (■) Outward current at the end of the +40 mV pulse, (○ and ●) peak inward current at end of the −120-mV pulse. (B and D) Traces a–c corresponding to times indicated in A and C. (E) Ca fluorescence in same oocyte shown in C and D. The oocyte was injected with Ca-green dextran and imaged by confocal microscopy during the +40-mV (■) and −120-mV (○) voltage-clamp pulses, as previously described (Machaca and Hartzell, 1999).

quence of Ca^{2+} release from internal stores. Opening these channels produces a transient depolarization of the egg cell membrane (the "fertilization potential") to prevent polyspermy (the so-called "fast block to polyspermy") (Webb and Nuccitelli, 1985; Jaffe and Cross, 1986; Fontanilla and Nuccitelli, 1998). Our data predicts that increases in $[Ca^{2+}]$ above 1 μM would be required to produce the fertilization potential because the strong outward rectification of the Cl^- current at lower $[Ca^{2+}]$ would strongly limit the inward current required for depolarization. This expectation is supported by measurements showing that $[Ca^{2+}]$ at the membrane reaches ~1.2 μM after fertilization (Fontanilla and Nuccitelli, 1998). Because the membrane potential of the egg is determined almost entirely by Cl^- conductance, the voltage-dependent Ca^{2+} sensitivity of the Cl^- channels in the egg may serve the rather simple function of ensuring a high Ca^{2+} threshold for activation of the fast block to polyspermy. The fertilization potential is transient and lasts only ~15 min. As Ca^{2+} declines with time after fertilization, the outward rectification of the Ca^{2+}-activated Cl^- current may assist in repolarization of the membrane.

This difference in behavior of the channel at different $[Ca^{2+}]$ explains the complex behavior of Ca^{2+}-activated Cl^- currents in *Xenopus* oocytes, which we have previously described. We have previously shown (Hartzell, 1996; Kuruma and Hartzell, 1999; Machaca and Hartzell, 1999) that there are two different macroscopic currents in these cells. One current (I_{Cl2}) is activated selectively by Ca^{2+} influx, whereas the other ($I_{Cl1\text{-}S}$ and $I_{Cl1\text{-}T}$) is activated both by influx and release of Ca^{2+} from stores. We have confirmed that in oocytes without a vitelline membrane, these same currents develop in response to IP_3 injection (data not shown). Although we have been ambivalent as to whether these different macroscopic currents are mediated by the same or different types of channels, we now feel confident that we can explain the currents by a single species of channel that is gated by the mechanisms described in this paper. The combination of different Ca^{2+} concentrations provided by Ca^{2+} released from stores (lower concentration) and Ca^{2+} influx (higher concentration) coupled with the voltage sensitivity of the channel at low $[Ca^{2+}]$ can generate complex mac-

roscopic currents. This adds a new dimension to how Ca^{2+} signals may be interpreted by cells.

In excitable cells where the membrane potential regularly oscillates above and below E_{Cl} due to other conductances, these different behaviors of Ca^{2+}-activated Cl^- channels at different [Ca^{2+}] could have very interesting consequences. For example, in some species, such as rabbit, an outward Ca^{2+}-activated Cl^- current normally plays a role in phase 1 repolarization of the cardiac action potential (Zygmunt and Gibbons, 1992; Zygmunt, 1994; Papp et al., 1995). However, under conditions of Ca^{2+} overload, this same channel may produce transient inward currents that are arrhythmogenic (January and Fozzard, 1988; Berlin et al., 1989; Zygmunt et al., 1998). This Ca^{2+}-activated Cl^- channel in rabbit heart has many features including single channel conductance (Collier et al., 1996) and anionic selectivity (Kawano et al., 1995) in common with the *Xenopus* oocyte channel. Thus, the voltage and Ca^{2+} sensitivity of Ca^{2+}-activated Cl^- channels place these channels in a pivotal role for regulation of cellular excitability.

We thank Dr. Steve Traynelis for extensive madvice and discussion and for help with the modeling in Fig. 14, and we thank Drs. Anant Parekh, Rick Aldrich, Nael McCarty, Shawn Zeltwanger, Khaled Machaca, and Jonathan Davis for comments on the manuscript and helpful discussion. We also thank Elizabeth Lytle and Alyson Ellingson for expert technical assistance.

Supported by National Institutes of Health grant RO1 GM 55276.

Submitted: 27 August 1999
Revised: 17 November 1999
Accepted: 18 November 1999
Released online: 28 December 1999

REFERENCES

Anderson, M., and M. Welsh. 1998. Calcium and cAMP activate different chloride channels in the apical membrane of normal and cystic fibrosis epithelia. *Proc. Natl. Acad. Sci. USA.* 88:6003–6007.

Arreola, J., J.E. Melvin, and T. Begenisich. 1996. Activation of calcium-dependent chloride channels in rat parotid acinar cells. *J. Gen. Physiol.* 108:35–47.

Arreola, J., J.E. Melvin, and T. Begenisich. 1998. Differences in regulation of Ca^{2+}-activated Cl^- channels in colonic and parotid secretory cells. *Am. J. Physiol.* 274:C161–C166.

Bajzer, E., A.C. Myers, S.S. Sedarous, and F.G. Prendergast. 1989. Pade-Laplace method for analysis of fluorescence intensity decay. *Biophys. J.* 56:79–93.

Barnes, S., and M.C. Deschenes. 1992. Contribution of Ca and Ca-activated Cl channels to regenerative depolarization and membrane bistability of cone photoreceptors. *J. Neurophysiol.* 68:745–755.

Berlin, J.R., M.B. Cannell, and W.J. Lederer. 1989. Cellular origins of the transient inward current in cardiac myocytes. Role of fluctuations and waves of elevated intracellular calcium. *Circ. Res.* 65: 115–126.

Bers, D.M., C. Patton, and R. Nuccitelli. 1994. A practical guide to the preparation of Ca^{2+} buffers. *Methods Cell Biol.* 40:3–29.

Boton, R., N. Dascal, B. Gillo, and Y. Lass. 1989. Two calcium-activated chloride conductances in *Xenopus laevis* oocytes permeabilized with the ionophore A23187. *J. Physiol.* 408:511–534.

Braun, A.P., and H. Schulman. 1995. A non-selective cation current activated via the multifunctional Ca^{2+}-calmodulin-dependent protein kinase in human epithelial cells. *J. Physiol.* 488:37–55.

Chan, H.C., M.A. Kaetzel, A.L. Gotter, J.R. Dedman, and D.J. Nelson. 1994. Annexin IV inhibits calmodulin-dependent protein kinase II-activated chloride conductance. A novel mechanism for ion channel regulation. *J. Biol. Chem.* 269:32464–32468.

Chao, A.C., K. Kouyama, E.K. Heist, Y.-J. Dong, and P. Gardner. 1995. Calcium- and CaMKII-dependent chloride secretion induced by the microsomal Ca^{2+}-ATPase inhibitor 2,5-Di-(tert-butyl)-1,4-hydroquinone in cystic fibrosis pancreatic epithelial cells. *J. Clin. Invest.* 96:1794–1801.

Clarke, L.L., B.R. Grubb, J.R. Yankaskas, C.U. Cotton, A. McKenzie, and R.C. Boucher. 1994. Relationship of a non–cystic fibrosis transmembrane conductance regulator-mediated chloride conductance to organ-level disease in Cftr(−/−) mice. *Proc. Natl. Acad. Sci. USA.* 91:479–483.

Cliff, W.H., and R.A. Frizzell. 1990. Separate Cl conductances activated by cAMP and Ca in Cl secreting epithelial cells. *Proc. Natl. Acad. Sci. USA.* 87:4956–4960.

Collier, M.L., P.C. Levesque, J.L. Kenyon, and J.R. Hume. 1996. Unitary Cl^- channels activated by cytoplasmic Ca^{2+} in canine ventricular myocytes. *Circ. Res.* 78:936–944.

Cui, J., D.H. Cox, and R.W. Aldrich. 1997. Intrinsic voltage dependence and Ca^{2+} regulation of mslo large conductance Ca-activated K^+ channels. *J. Gen. Physiol.* 109:647–673.

Cunningham, S.A., M.S. Awayda, J.K Bubien, I.I. Ismailov, M.P. Arrate, B.K. Berdiev, D.J. Benos, and C.M. Fuller. 1995. Cloning of an epithelial chloride channel from bovine trachea. *J. Biol. Chem.* 270:31016–31026.

Dascal, N. 1987. The use of *Xenopus* oocytes for the study of ion channels. *CRC Crit. Rev. Biochem.* 22:317–387.

DeCastro, F., E. Geijo-Barrientos, and R. Gallego. 1997. Calcium-activated chloride current in normal mouse sympathetic ganglion cells. *J. Physiol.* 498:397–408.

Fine, B.P., E.S. Marques, and K.A. Hansen. 1994. Calcium-activated sodium and chloride fluxes modulate platelet volume: role of Ca^{2+} stores. *Am. J. Physiol.* 267:C1435–C1441.

Fontanilla, R.A., and R. Nuccitelli. 1998. Characterization of the sperm-induced calcium wave in *Xenopus* eggs using confocal microscopy. *Biophys. J.* 75:2079–2087.

Freeman, L.C., L.M. Pacioretty, N.S. Moise, R.S. Kass, and R.E. Gilmour, Jr. 1997. Decreased density of I(to) in left ventricular myocytes from German shepherd dogs with inherited arrhythmias. *J. Cardiovasc. Electrophysiol.* 8:872–883.

Frizzell, R.A., G. Rechkemmer, and R.L. Shoemaker. 1986. Altered regulation of airway epithelial cell chloride channels in cystic fibrosis. *Science.* 233:558–560.

Gomez-Hernandez, J.-M., W. Stühmer, and A.B. Parekh. 1997. Calcium dependence and distribution of calcium-activated chloride channels in *Xenopus* oocytes. *J. Physiol.* 502:569–574.

Gray, M.A., J.P. Winpenny, B. Verdon, H. McAlroy, and B.E. Argent. 1995. Chloride channels and cystic fibrosis of the pancreas. *Biosci. Rep.* 15:531–541.

Grubb, B.R., R.N. Vick, and R.C. Boucher. 1994. Hyperabsorption of Na^+ and raised Ca^{2+}-mediated Cl^- secretion in nasal epithelia of CF mice. *Am. J. Physiol.* 266:C1478–C1483.

Gruber, A.D., R.C. Elble, H.-L. Ji, K.D. Schreur, C.M. Fuller, and B.U. Pauli. 1998. Genomic cloning, molecular characterization, and functional analysis of human CLCA1, the first human member of the family of Ca^{2+}-activated Cl channel proteins. *Genomics.* 54:200–214.

Han, X., and G.R. Ferrier. 1992. Ionic mechanisms of transient inward current in the absence of Na^+–Ca^{2+} exchange in rabbit cardiac Purkinje fibres. *J. Physiol.* 456:19–38.

Han, X., and G.R. Ferrier. 1996. Transient inward current is conducted through two types of channels in cardiac Purkinje fibres. *J. Mol. Cell. Cardiol.* 28:2069–2084.

Hartzell, H.C. 1996. Activation of different Cl currents in *Xenopus* oocytes by Ca liberated from stores and by capacitative Ca influx. *J. Gen. Physiol.* 108:157–175.

Hille, B. 1992. Ion Channels of Excitable Membranes. Sinauer Associates, Inc., Sunderland, MA. 341–344.

Jaffe, L.A., and N.L. Cross. 1986. Electrical regulation of sperm–egg fusion. *Ann. Rev. Physiol.* 48:191–200.

January, C.T., and H.A. Fozzard. 1988. Delayed afterdepolarizations in heart muscle: mechanisms and relevance. *Pharmacol. Rev.* 40: 219–227.

Jentsh, T., and W. Gunther. 1997. Chloride channels, an emerging molecular picture. *Bioessays.* 19:117–126.

Ji, H., M.D. Duvall, H.K. Patton, C.L. Satterfield, C.M. Fuller, and D.J. Benos. 1998. Functional expression of a truncated Ca activated Cl channel and activation by phorbol ester. *Am. J. Physiol.* 455–464.

Johnson, L.G., S.E. Boyles, J. Wilson, and R.C. Boucher. 1995. Normalization of raised sodium absorption and raised calcium-mediated chloride secretion by adenovirus-mediated expression of cystic fibrosis transmembrane conductance regulator in primary human cystic fibrosis airway epithelial cells. *J. Clin. Invest.* 95: 1377–1382.

Kawano, S., Y. Hirayama, and M. Hiraoka. 1995. Activation mechanism of Ca^{2+}-sensitive transient outward current in rabbit ventricular myocytes. *J. Physiol.* 486:593–604.

Klöckner, U. 1993. Intracellular calcium ions activate a low-conductance chloride channel in smooth muscle cells isolated from human mesenteric artery. *Pflügers Arch.* 424:231–237.

Kurahashi, T., and K.-W. Yau. 1994. Olfactory transduction. Tale of an unusual chloride current. *Curr. Biol.* 4:256–258.

Kuruma, A., and H.C. Hartzell. 1999. Dynamics of calcium regulation of Cl currents in *Xenopus* oocytes. *Am. J. Physiol.* 276:C161–C175.

Kuruma, A., M. Hiraoka, and S. Kawano. 1998. Activation of Ca^{2+}-sensitive Cl^- current by reverse mode Na^+/Ca^{2+} exchange in rabbit ventricular myocytes. *Pflügers Arch.* 436:976–983.

Large, W.A., and Q. Wang. 1996. Characteristics and physiological role of the Ca^{2+}-activated Cl^- conductance in smooth muscle. *Am. J. Physiol.* 271:C435–C454.

Machaca, K., and H.C. Hartzell. 1998. Asymmetrical distribution of Ca-activated Cl channels in *Xenopus* oocytes. *Biophys. J.* 74:1286–1295.

Machaca, K., and H.C. Hartzell. 1999. Reversible Ca gradients between the sub-plasmalemma and cytosol differentially activate two distinct Cl channel effectors. *J. Gen. Physiol.* 113:249–266.

Martin, D.K. 1993. Small conductance chloride channels in acinar cells from rat mandibular salivary gland are directly controlled by a G-protein. *Biochem. Biophys. Res. Commun.* 192:1266–1273.

Marty, A., Y.P. Tan, and A. Trautmann. 1984. Three types of calcium-dependent channel in rat lacrimal glands. *J. Physiol.* 357: 293–325.

Marunaka, Y., and D.C. Eaton. 1990. Effects of insulin and phosphatase on a Ca^{2+}-dependent Cl^- channel in a distal nephron cell line (A6). *J. Gen. Physiol.* 95:773–789.

Morris, A.P. 1999. The regulation of epithelial cell cAMP- and calcium-dependent chloride channels. *Adv. Pharmacol.* 46:209–251.

Morris, A.P., and R.A. Frizzell. 1993. Ca^{2+}-dependent Cl^- channels in undifferentiated human colonic cells (HT-29). II. Regulation and rundown. *Am. J. Physiol.* 264:C977–C985.

Naranjo, D., and P. Brehm. 1993. Modal shifts in acetylcholine receptor channel gating confer subunit-dependent desensitization. *Science.* 260:1811–1814.

Neher, E. 1992. Correction for liquid junction potentials in patch clamp experiments. *Methods Enzymol.* 207:123–131.

Nelson, M.T., M.A. Conway, H.J. Knot, and J.E. Brayden. 1997. Chloride channel blockers inhibit myogenic tone in rat cerebral arteries. *J. Physiol.* 502:259–264.

Nilius, B., J. Prenen, G. Szucs, L. Wei, F. Tanzi, T. Voets, and G. Droogmans. 1997a. Calcium-activated chloride channels in bovine pulmonary artery endothelial cells. *J. Physiol.* 498:381–396.

Nilius, B., J. Prenen, T. Voets, K. Van Den Bremt, J. Eggermont, and G. Droogmans. 1997b. Kinetic and pharmacological properties of the calcium-activated chloride-current in microvascular endothelial cells. *Cell Calc.* 22:53–63.

Nishimoto, I., J. Wagner, H. Schulman, and P. Gardner. 1991. Regulation of Cl^- channels by multifunctional CaM kinase. *Neuron.* 6:547–555.

Papp, Z., K. Sipido, G. Callewaert, and E. Carmeliet. 1995. Two components of $[Ca^{2+}]_i$-activated Cl^- current during large $[Ca^{2+}]_i$ transients in single rabbit heart Purkinje cells. *J. Physiol.* 483:319–330.

Schlenker, T., and J.G. Fitz. 1996. Ca^{2+}-activated Cl^- channels in human biliary cell line: regulation by Ca^{2+}/calmodulin-dependent protein kinase. *Am. J. Physiol.* 271:G304–G310.

Schumann, M.A., P. Gardner, and T.A. Raffin. 1993. Recombinant human tumor necrosis factor alpha induces calcium oscillation and calcium-activated chloride current in human neutrophils. The role of calcium/calmodulin-dependent protein kinase. *J. Biol. Chem.* 268:2134–2140.

Takahashi, T., E. Neher, and B. Sakmann. 1987. Rat brain serotonin receptors in *Xenopus* oocytes are coupled by intracellular calcium to endogenous channels. *Proc. Natl. Acad. Sci. USA.* 84:5063–5067.

Taleb, O., P. Feltz, J.-L. Bossu, and A. Feltz. 1988. Small-conductance chloride channels activated by calcium on cultured endocrine cells from mammalian pars intermedia. *Pflügers Arch.* 412: 641–646.

Taleb, O., J. Trouslard, B.A. Demeneix, P. Feltz, J.-L. Bossu, J.-L. Dupont, and A. Feltz. 1987. Spontaneous and GABA-evoked chloride channels on pituitary intermediate lobe cells and their internal Ca requirements. *Pflügers Arch.* 409:620–631.

Tohda, M., J. Nakamura, H. Hidaka, and Y. Nomura. 1991. Inhibitory effects of KN-62, a specific inhibitor of Ca/calmodulin-dependent protein kinase II, on serotonin-evoked C1-current and 36-C1-efflux in *Xenopus* oocytes. *Neurosci. Lett.* 129:47–50.

Tsien, R.Y., and T. Pozzan. 1989. Measurements of cytosolic free Ca^{2+} with Quin-2. *Methods Enzymol.* 172:230–262.

VanRenterghem, C., and M. Lazdunski. 1993. Endothelin and vasopressin activate low conductance chloride channels in aortic smooth muscle. *Pflügers Arch.* 425:156–163.

Wagner, J.A., A.L. Cozens, H. Schulman, D.C. Gruenert, L. Stryer, and P. Gardner. 1991. Activation of chloride channels in normal and cystic fibrosis airway epithelial cells by multifunctional calcium/calmodulin-dependent protein kinase. *Nature.* 349:793–796.

Wang, Y.X., and M.I. Kotlikoff. 1997. Inactivation of calcium-activated chloride channels in smooth muscle by calcium/calmodulin-dependent protein kinase. *Proc. Natl. Acad. Sci. USA.* 94: 14918–14923.

Wang, Z., B. Fermini, J. Feng, and S. Nattel. 1995. Role of chloride currents in repolarizing rabbit atrial myocytes. *Am. J. Physiol.* 268: H1992–H2002.

Webb, D., and R. Nuccitelli. 1985. Fertilization potential and electrical properties of the *Xenopus laevis* egg. *Dev. Biol.* 107:395–406.

Worrell, R.T., and R.A. Frizzell. 1991. CaMKII mediates stimulation of chloride conductance by calcium in T84 cells. *Am. J. Physiol.* 260:C877–C882.

Wright, E.M., and J.M. Diamond. 1977. Anion selectivity in biological systems. *Physiol. Rev.* 57:109–156.

Xie, W., M.A. Kaetzel, K.S. Bruzik, J.R. Dedman, S.B. Shears, and D.J. Nelson. 1996. Inositol 3,4,5,6-tetrakisphosphate inhibits the calmodulin-dependent protein kinase II-activated chloride conductance in T84 colonic epithelial cells. *J. Biol. Chem.* 271:14092–14097.

Yao, Y., and I. Parker. 1993. Inositol trisphosphate–mediated Ca^{2+} influx into *Xenopus* oocytes triggers Ca^{2+} liberation from intracellular stores. *J. Physiol.* 468:275–296.

Yeramian, E., and P. Claverie. 1987. Analysis of multi-exponential functions without a hypothesis as to the number of components. *Nature.* 326:169–174.

Yuan, X.J. 1997. Role of calcium-activated chloride current in regulating pulmonary vasomotor tone. *Am. J. Physiol.* 272:L959–L968.

Zygmunt, A. and W.R. Gibbons. 1992. Properties of the calcium-activated chloride current in heart. *J. Gen. Physiol.* 99:391–414.

Zygmunt, A.C. 1994. Intracellular calcium activates a chloride current in canine ventricular myocytes. *Am. J. Physiol.* 267:H1984–H1995.

Zygmunt, A.C., and W.R. Gibbons. 1991. Calcium-activated chloride current in rabbit ventricular myocytes. *Circ. Res.* 68:424–437.

Zygmunt, A.C., R.J. Goodrow, and C.M. Weigel. 1998. I_{NaCa} and $I_{Cl(Ca)}$ contribute to isoproterenol-induced afterhyperpolarizations in midmyocardial cells. *Am. J. Physiol.* 275:H1979–H1992.